Head-Disk Interface Dynamic Instability due to Intermolecular Forces

Brian H. Thornton and David B. Bogy

Computer Mechanics Laboratory
5129 Etcheverry Hall
Department of Mechanical Engineering
University of California
Berkeley, CA. 94720

ABSTRACT – This paper presents a nonlinear dynamic analysis of the head-disk interface by including intermolecular adhesion forces for sub- 5 nm flying air bearing sliders. Experimental evidence shows that one of the major roadblocks in achieving ultra-low flying-heights is the stability of the head-disk interface. It is found that the inclusion of intermolecular forces between the slider and disk in modeling the head-disk interface leads to dynamic instability of the slider. It is shown by a bifurcation diagram that a slider can easily be forced into unstable, high amplitude oscillations. It is also shown that the experimentally observed spin-down – spin-up flying-height hysteresis, intermittent flying instability, and "snapping" from stable to unstable proximity can be explained by the inclusion of the intermolecular forces. A parametric study is conducted showing the dependence of stability/instability on the variables. By understanding the effect each parameter has on stability, we can achieve air bearing surface and disk morphology system design guidelines. From this study it is found that the head-disk interface can become unstable due to intermolecular forces below a flying-height of about 6 nm. However, from the results of the parametric study, it is shown that a head-disk interface can be designed such that it maximizes stability, although the instability cannot be attenuated completely. By minimizing the intermolecular adhesion forces and the flying-height modulation, and by maximizing the air bearing stiffness and damping, we achieve maximum stability. Also, it is found that the stiffening effect of the air bearing film increases the stability. The implications of this study are that the head-disk interface stability is dramatically compromised in the sub- 6 nm flying-height regime and that the glide-height of "super-smooth" disks will not only be a function of the disk's morphology but also the intermolecular adhesion force induced instability of the slider.

INTRODUCTION

In order to achieve a magnetic recording areal density of 1 Tbit/in^2 it is expected that the physical spacing between the media and transducer or flying-height (FH) will have to be 3.5 nm [1]. For a head-disk interface (HDI) to perform reliably, both tribologically and magnetically, the fluctuations in the FH must be held to a minimum. One of the roadblocks thus far for realizing a 3.5 nm FH is the dynamic stability of the HDI. It has been seen experimentally that a slider can transition from stable to unstable proximity flying by decreasing the FH only slightly [2]. Also, it has been widely observed that a slider's touchdown and takeoff FH's are not equal. This "snapping" effect between stability and instability and the difference in a slider's touchdown and takeoff FH's are evidence of a complicated dynamical system when operating in the sub- 6 nm FH regime. As the slider and disk spacing is decreased, the interface surface interactions are evidently no longer negligible. Two adhesion models have been proposed to account for the interactions between the slider and the disk: one is based on lubricant interacting with the slider causing a meniscus force and the other is based on intermolecular forces between the two intimate surfaces.

Previous publications have studied the effects of lubricant on HDI stability and flying characteristics [3] - [6]. Kato *et. al.* used an equilibrium meniscus force model in simulations to account for the dynamic slider-lubricant interactions [4] - [6]. However, their use of this meniscus force model neglects some very important assumptions of the model: extremely thin liquid lubricant film thickness (> 15 Å) and the kinetic formation of a meniscus. Generally, lubricant is highly bonded to the disk surface, thus only a fraction of the lubricant layer is available to behave as a liquid in the formation of a

meniscus making a meniscus more energetically difficult to form. Also, on the time scale of interest for "bouncing" or unstable proximity of the air bearing slider, the liquid volume required to form the meniscus does not have time to be transported and is far from the equilibrium state according to a kinetic meniscus formation model [7].

Intermolecular adhesion forces can be extremely large when two very flat surfaces come within proximity. In fact, it has been shown that intermolecular adhesion forces is the mechanism that allows gecko lizards to "stick" on molecularly smooth surfaces [8]. Therefore, when flying an extremely smooth air bearing slider over a "super-smooth" disk at ultra-low FH's, intermolecular forces must be accounted for. Thus far, publications investigating the effect of intermolecular forces on the HDI have been based on static analysis [9] - [11]. It has been shown that for air bearing sliders flying in the sub- 5 nm regime, intermolecular forces can become important and cause a significant decrease in static FH [9]. However, the implications of intermolecular forces on the dynamic stability of the HDI have not been published.

In this paper we present some experimental evidence of the abrupt stable to unstable flying transition and the FH hysteresis, which are measures of instability for the HDI. We also show that even for non-lubricated disks HDI instability occurs, suggesting this phenomenon is more likely to be caused by intermolecular forces than by meniscus forces. By accounting for the intermolecular forces through a Lennard-Jones potential and modeling the HDI as a lumped parameter one degree-of-freedom (1DOF) model, we show that the system becomes highly nonlinear in the proximity region. It is shown that the dynamics of this nonlinear system are extremely complicated and can even be chaotically unstable. From a nonlinear dynamics analysis with nominal values and from a

parametric study, the variables implicating the HDI stability/instability are discussed including design guidelines to minimize HDI instability due to intermolecular forces.

EXPERIMENTAL RESULTS

It has been observed that when the FH of a slider is gradually reduced to within proximity of an extremely "super-smooth" disk the slider can be easily set into unstable high amplitude oscillations. Figure 1a shows the absolute displacement of the trailing edge center of slider 2 shown in Fig. 2 flying in proximity of the disk at linear velocities of 3.6, 3.4 and 3.2 m/s. This result is measured by a laser Doppler vibrometer (LDV) in the bandwidth of 10kHz – 2 MHz. It is seen that the slider transitions abruptly from stable to intermittently unstable and then further to indefinitely unstable as the velocity is lowered slightly. The high amplitude oscillations of the slider appear to be self-excited as opposed to asperity contact induced. This "snapping" effect from stable to unstable suggests complex dynamics of the HDI system.

It has been widely observed that as a slider is forced into and back out of contact by decreasing and increasing disk speed or pressure, a FH hysteresis is present (i.e., touchdown FH ≠ takeoff FH) [12]. Experiments investigating HDI instabilities as a function of the FH were conducted on a TTi T1000 spinstand for various sliders and disks while controlling the FH with the spindle speed of the disk. The sliders instability and contact was initially measured by both LDV and an acoustic emission (AE) sensor, however, the LDV was found to be much more sensitive than the AE sensor. Therefore, the sliders vertical motion was measured by a LDV and highpass filtered at 60 kHz to obtain air bearing resonance vibration and slider body vibration modes to detect unsteady proximity and contact, respectively. This signal was then acquired through a RMS circuit

sampled at 4 kHz. A typical FH hysteresis can be seen in Fig. 1b, which shows the sliders RMS vertical velocity as the disk spindle RPM is lowered until the slider comes into unsteady proximity and/or contact with the disk (touchdown) and then the disk spindle RPM is increased and the slider ceases to contact and flies in steady proximity over the disk (takeoff). It has been observed that the touchdown RPM is lower than the takeoff RPM or the touchdown height (TDH) is less than the takeoff height (TOH). This difference in RPM or FH is what constitutes this hysteresis (TOH - TDH). Several sets of experiments were conducted using four different sub-ambient pressure pico sliders and a set of disks with varying lubricant thickness. The four air bearing surfaces (ABS) are shown in Fig. 2. Two types of disks were used in this experiment: B2 with R_a = 0.3 nm and B4 with R_a = 0.2 nm both with glide-heights of 2.5 to 4 nm. The disks were all processed in exactly the same manner with the only variation being the lubricant thickness: 0 (not lubricated), 8, 12, 16 and 20 Å. The lubricant is a perfluoropolyether (PFPE) with a high bonding ability to the disk of approximately 80%. For every test, new samples were used so as to not affect the experimental results by lubricant pickup on the slider, wear and other factors. Figures 3 through 6 summarize the experimental results for sliders 1 – 4. The bar graphs show the touchdown, takeoff, and hysteresis RPM's as a function of lubricant thickness. It is interesting to notice that for all of the lubricant thicknesses tested, there is no trend in the FH hysteresis as a function of lubricant thickness. What is common among all the tests is that a FH hysteresis is present for all disks and sliders tested including the non-lubricated disks and that the takeoff RPM was always higher than the touchdown RPM. This FH hysteresis can be used as a measure of instability of the HDI. For example, take the case of slider 3 flying over the disk with 0 Å

of lubricant (see Fig. 5). If the slider is flying at any speed between 3500 RPM (touchdown) and 8000 RPM (takeoff) the slider has the ability to become unstable and remain unstable until the RPM is increased beyond the 8000 RPM (takeoff). Also, the intensity of the sliders vibration can be measured from the RMS value of the LDV signal. For sliders 1 – 3, the intensity of vibration saturated the data acquisition system. However, slider 4 exhibited very low vibration amplitude, as seen in Fig. 7 compared to the other sliders. The main difference between sliders 1 –3 and 4 is the small diamond-like carbon pads distributed across the entire ABS. These small pads on slider 4 decrease the actual proximity/contact area substantially and lead to less adhesion force, which could explain the results seen in Fig. 7. Also, the sliders vibration amplitude in Fig. 1b is asymmetric, showing that the maximum slider vibration does not occur when the RPM is the lowest.

Both the "snapping" effect from steady to unsteady proximity flying and the presence of a FH hysteresis are new phenomena not well understood. By simulating a quasi-static FH and the touchdown-takeoff process, accounting for all of the forces shown in the free-body diagram in Fig. 8, we would not predict this "snapping" effect from stable to unstable proximity or the FH hysteresis. Therefore to explain the above experimental observations, it appears that additional forces at the HDI can no longer be neglected for such low FH's.

ADHESION FORCES AT THE HDI

With FH's decreasing and the probability of contact increasing, a better understanding of the interface interactions are becoming more important in developing a reliable HDI. Also, with the intimate surfaces of the slider and disk becoming extremely

smooth (i.e., close to atomically smooth) and with the presence of a thin layer of lubricant on the disk surface, the interface interactions become very complicated. Generally the interface is a diamond-like carbon (DLC) coated slider surface – the air – a lubricant interface during flying, and a DLC coated slider surface – lubricant surface interface during contact. If the disk is not lubricated, the interface would include the DLC coated disk instead of the lubricant layer. The source and nature of the interface forces acting between the slider and the disk can be very complicated. Such forces can be generated through electrostatic charging, tribocharging, and adhesion. In this paper we will only consider adhesion forces acting at the interface.

At least two types of adhesion forces can be generated at the HDI: capillary (meniscus) and intermolecular. In order for meniscus forces to be generated, a liquid layer must be present at the interface. In the case of the HDI, the liquid layer would consist of primarily the mobile lubricant and possibly a very thin condensed water vapor layer. Also, the formation of a meniscus force is kinetic, hence, highly time dependent [7]. It has been shown through experiments and simulation that the meniscus force is negligible when the slider and lubricant are in contact over a short enough time period and increases to a steady-state value over a time period on the order of minutes [7], [13]. Under dynamic instability of the slider, it can be seen from Fig. 1a that the slider is in contact with the lubricant layer for less than 800 ns; far too short to form a measurable meniscus force as predicted from a kinetic meniscus formation model and previous experimental results. Also, for the high velocity vibration of the slider under unstable proximity, it is still unknown if the lubricant behaves as a liquid or a solid when the slider impacts the lubricant. Our experimental results agree with the above analysis. If meniscus

forces were partially the cause of the additional interface forces, then we would expect the FH hysteresis to increase as the lubricant thickness increases, and little or no FH hysteresis should exist for an interface without lubricant. Our experimental results shown in Figs. 3 – 6, show no clear trend in the FH hysterisis with increasing lubricant thickness and that a FH hysterisis is present even for an interface without lubricant.

Other lubricant interactions could possibly cause new dynamic HDI phenomena; however, the above experimental results showed very little correlation between a meniscus force effect and instability. For the following analysis the contribution of adhesion due to meniscus formation under the unsteady proximity regime seems unlikely and adhesion due to intermolecular forces, which is time independent for unsteady proximity of the HDI, is considered to be the sole contributor to adhesion. To get an idea of the magnitude of the adhesion force generated by intermolecular forces we focus on a particular system. For a flat area, A_s = 15,000 μm^2 (approximate area of the alumina at the trailing edge of slider 2) placed parallel to a flat disk surface, the van der Waals intermolecular adhesion force as a function of separation distance, D, is [14]

$$F = \left(\frac{A}{6\pi D^3} \right) \cdot A_s \qquad (1)$$

where A is the Hamaker constant assumed to have a value between 0.4-4×10^{-19} J for condensed phases across air or vacuum [14]. Figure 9 shows the adhesion force as a function of separation distance for the range of Hamaker constants given above. It is seen that at a separation distance of 3 nm, the adhesion force can range from 0.12 – 1.2 gm, which is quite significant at the HDI. This example does not take into account the slider's attitude, crown, camber and twist or roughness effects. In the following analysis we

account for the slider geometry parameters and will comment on the effect of slider/disk roughness in the discussion section.

HEAD-DISK INTERFACE MODEL

A. Modeling Intermolecular Forces

For modeling of the intermolecular forces, we adopted the method of Lin and Bogy who implemented an additional force into the CML Static Air Bearing Simulation Code via the Lennard-Jones potential [9]. The Hamaker constant, *A*, was taken to be 10^{-19} *J* and the repulsion constant, *B*, was taken to be 10^{-76} Jm^6. This method takes the slider air bearing geometry and flying attitude into account, however, it assumes mathematically smooth surfaces. The fixed attitude solution is found by fixing the attitude of the slider (FH, pitch, and roll) and solving for the forces acting on the slider. When the forces and moments acting on the slider equal those of the suspension, the static solution is obtained. Figure 10a shows the resultant intermolecular force acting on the pico size ABS shown in Fig. 2 (slider 2) as a function of minimum FH for a roll angle of 1.5 μrad and pitch angle of 40 μrad; similar to the conditions under which slider 2 exhibits unstable proximity. It is seen that as the FH decreases, an attractive force becomes present around 5 nm and by further decreasing the FH, a strong repulsive force becomes present, as expected. The Lennard-Jones model does not allow for physical contact between the slider and disk. The Lennard-Jones modeled force becomes unbounded as the spacing goes to zero due to the repulsion term to simply model physical contact. This simplification in the repulsion term modeling physical contact will be commented on in the discussion section.

However, it will be shown that even though the Lennard-Jones repulsion and physical contact are modeled differently, they predict similar dynamic instability results.

B. Static Force Analysis

Figure 10b shows the resultant force exerted on the slider as a function of minimum FH for the fixed attitude solution. The force consists of the positive and negative (sub-ambient) air bearing forces and the adhesion and repulsion forces from the Lennard-Jones potential. When the intermolecular forces are accounted for there can exist up to three equilibria – two stable and one unstable. It is seen that for small perturbations about the nominal FH solution of 7 nm, the solution is stable. However, at 2.8 nm, there exists an unstable equilibrium and another stable equilibrium at 0.2 nm. These additional equilibria suggest a very complicated nonlinear system, which is the focus of the following dynamic analysis.

C. Nonlinear One Degree-of-Freedom HDI Model

In order to simplify the HDI for the following analysis, we used the simple lumped parameter 1DOF model depicted in Fig. 11. In this model, the air bearing slider system is modeled with a nonlinear spring, *k(s)*, mass, *m*, and proportional damping, *c*. The nonlinear air bearing stiffness is a function of the slider – disk spacing, *s*, and takes the power-hardening form

$$k(s) = b \cdot s^{a} \tag{2}$$

where α and β are constants found by matching with the CML dynamic simulation code [2]. The air bearing force can be found from

$$F_{ab}(x) = -k(s) \cdot x = -b \cdot (FH_{ss} + x - d)^{a} \cdot x \tag{3}$$

where FH_{ss} is the steady-state FH without accounting for the intermolecular force and x is the slider's absolute displacement: $x = s + d - FH_{ss}$. The disk topography, $d(t)$, can be modeled in various ways; as a numerically generated random wavy surface, a harmonic excitation, or using an experimentally measured disk topography. The intermolecular force, F_{vdW}, acting on the slider takes the form

$$F_{VdW}(s) = -\frac{A'}{s^3} + \frac{B'}{s^9} = -\frac{A'}{(FH_{ss} + x - d)^3} + \frac{B'}{(FH_{ss} + x - d)^9} \tag{4}$$

where A' and B' are constants found from curve fitting plots similar to Fig. 10a where the first term is the attraction force and the second term is the repulsion force. The equation of motion for this system can be written in terms of the sliders absolute displacement, x

$$m\ddot{x} + c\dot{x} + (k - F_{VdW})x + (F_{VdW} - k)d - c\dot{d} = 0 \tag{5}$$

Due to the intermolecular force in Eq. (4) and the nonlinear spring stiffness in Eq. (3), Eq. (5) becomes highly nonlinear, and due to the addition of the intermolecular force, the solution is not simple.

HEAD-DISK INTERFACE NONLINEAR ANALYSIS

A. Stability

Stability of the HDI model can be analyzed by considering the energy of the system. If we assume no forcing, $d(t) = 0$, and no damping, $c = 0$, the system is conservative and a potential energy method can be used to show equilibria and local stability. The potential energy of the system, U_{sys}, is comprised of the potential energy of the air bearing spring, U_{ab}, and the potential energy of the intermolecular force, U_{vdW},

derived from the Lennard-Jones potential. These conservative forces are related to their potential energies through

$$F(x) = -\frac{\partial U}{\partial x} \tag{6}$$

The total potential energy can be found by integrating the air bearing force, F_{ab}, and the intermolecular force, F_{vdW}

$$U_{sys} = U_{ab} + U_{vdW} = -\left[\int F_{ab}dx + \int F_{VdW}dx\right] =$$
$$-\left[\int -\left(b\left(FH_{ss} + x\right)^{a} x\right)dx + \int\left(-\frac{A'}{\left(FH_{ss} + x\right)^{3}} + \frac{B'}{\left(FH_{ss} + x\right)^{9}}\right)dx\right] \tag{7}$$

The criteria for equilibrium, x_i^*, is satisfied when the system's potential reaches an inflection point

$$\frac{\partial U_{sys}}{\partial x} = 0 \tag{8}$$

and the equilibrium point is stable if the potential evaluated at equilibrium is a local minimum

$$\left.\frac{\partial^2 U_{sys}}{\partial x^2}\right|_{x_i^*} > 0 \tag{9}$$

and is unstable if the potential evaluated at equilibrium is a local maximum

$$\left.\frac{\partial^2 U_{sys}}{\partial x^2}\right|_{x_i^*} < 0 \tag{10}$$

For the nominal coefficients used, as shown in Table 1, equilibria and stability as a function of FH_{ss} can be obtained. Figure 12 shows the potential energies of the air bearing, the Lennard-Jones potential and the total system potential at FH_{ss} = 7.75 nm as a

function of spacing. It is seen when the air bearing and the Lennard-Jones potentials are added, the system has one equilibrium, FH_{eq}, and it is stable, where $FH_{eq} = x_i^* + FH_{ss}$. In Fig. 13, the total potentials for FH_{ss} = 7.75, 5.75, 4.75, and 1.25 nm are shown as a function of spacing. It is seen, at FH_{ss} of 7.75 nm, one stable equilibrium exists at FH_{eq} = 7.75 nm. At FH_{ss} = 5.75 nm, there exists two stable and one unstable equilibria at FH_{eq} = 5.75, 0.35, and 0.7 nm, respectively. At FH_{ss} = 1.25 nm, the air bearing is overcome by the intermolecular force and only one stable equilibrium exists, FH_{eq} = 0.25 nm. The equilibria and stability as a function of FH_{ss} can be summarized in the bifurcation plot shown in Fig. 14. It is seen that when FH_{ss} is greater than 6.3 nm only one equilibrium exists, x_1^*, the nominal FH solution. Between FH_{ss} of 1.35 nm and 6.3 nm, three equilibria exist – two stable, x_1^* and x_3^* and one unstable, x_2^*. At FH_{ss} of 1.35 nm, only one stable equilibrium exists, x_3^*. The regime where the three equilibria exist is of utmost interest – both theoretically and for practical application.

Between FH_{ss} of 1.35 nm and 6.3 nm in Fig. 14 three equilibria exist and within this regime the potential energy takes on a special form generally called a “double-well” or “two-well” potential. Double-well potential systems have been studied for the past two decades in the field of nonlinear dynamics [15] - [18]. Many systems have exhibited double-well potentials with very interesting dynamics, from mechanical systems to super conductivity. Within this regime, the dynamics of the system are extremely complex and can even be chaotic [15] - [18]. A detailed nonlinear dynamics analysis of this system investigating periodic solutions, limit cycles, and transitions to chaos are interesting to study, however, the practical issues associated with the HDI would be over shadowed in

such a complete study. The details concerning the HDI stability and instability are of more interests to us here, and they are discussed in detail.

B. Unforced System

This system is considered to be unforced when the disk forcing is zero, $d(t) = 0$ (e.g. for a perfectly smooth disk surface). From the bifurcation plot in Fig. 14 we observe one very important characteristic of the unforced system. This observation can be explained by a touchdown (TD) – takeoff (TO) simulation by decreasing and then increasing the FH_{ss}. From Fig. 14, the FH_{eq}'s can be found as a function of FH_{ss} as the FH_{ss} is lowered from 10 nm to 1 nm and then increased back to 10 nm. As the FH_{ss} is decreased from 10 nm to 1.35 nm, the equilibrium follows the nominal solution, x_1^* (a-b). However, at the FH_{ss} of 1.35 nm, the air bearing is overcome by the intermolecular force and the nominal solution is annihilated by x_2^* and the slider "snaps" down to the other stable equilibrium, x_3^* (b-c). Upon increasing the FH_{ss} back to 10 nm, the equilibrium solution will remain along x_3^* until it is annihilated by x_2^*, at a FH_{ss} of 6.3 nm (d-e). At FH_{ss} = 6.3 nm the equilibrium solution "snaps" from x_3^* to x_1^*, back to the nominal solution (e-f). This is illustrated in Fig. 15, which depicts an unforced TD – TO simulation showing the slider remaining "stuck" on the disk until the FH_{ss} reaches 6.3 nm. The difference between the FH_{ss} at which the slider becomes "stuck" while decreasing the FH_{ss} and where the slider becomes "unstuck" while increasing the FH_{ss} is the unforced "FH hysteresis". It is seen that for the unforced system the FH hysteresis is bound by the regime were multiple equilibria exist – namely the three equilibria, x_1^*, x_2^*, and x_3^*.

Figure 16 shows a sketch of the energy surface in state-space (x versus $\dot{x}$) and the trajectories projected onto the state-space within the regime where the multiple equilibria exist, 1.35 < FH_{ss} < 6.3 nm. Since the unforced and undamped system is conservative, the systems trajectory remains on a level contour of the energy surface. Depending on the initial conditions the system will behave differently. In Fig. 16b, it is seen that for a relatively low energy state, $E < E_2$, with initial conditions near x_3^* or x_1^*, the slider oscillates about x_3^* or x_1^*, respectively, with small amplitudes. However, if enough initial energy is applied, $E > E_2$ the system remains in high amplitude oscillations about both x_1^* and x_3^*. The energy state that separates the oscillations about x_1^* or x_3^* and oscillations about both x_1^* and x_3^*, E_2, is defined as the homoclinic orbit or separatrix shown in Fig. 16. By adding damping, c, the systems trajectory would end up spiraling down into either x_1^* or x_3^* depending on the initial conditions as seen in Fig. 17. Two sets of initial conditions were chosen to illustrate the sensitivity to initial conditions: *(FH , velocity) = (6.3 nm , -0.3945 mm/s)* and *(FH , velocity) = (6.3 nm , -0.394 mm/s)*. It is seen that one of the trajectories spirals into x_1^* and the other spirals into x_3^*. The dynamics associated with the unforced system are rather simple as described above. However, once this type of system is forced, the sliders response becomes very nontrivial and highly unpredictable.

C. Forced System

Forced double-well potential systems have been found to exhibit *strange attractors* causing chaos and sensitivity to initial conditions; however, the important result for the HDI can be summarized as follows [15] - [18]. As long as the model of the HDI exhibits a double-well potential the forced solution can be periodic, non-periodic, or

chaotic for simple harmonic forcing. The homoclinic energy level separating oscillations about x_1^* or x_3^* and x_1^* and x_3^* can no longer be used to approximately predict the slider's response. That is, for the nominal parameters used, this system can exhibit non-predictable chaotic dynamics between FH_{ss} of 1.35 nm and 6.3 nm. The slider motion is defined as *stable* if it oscillates about the x_1^* equilibrium and *unstable* of all other motions. This choice of terminology describes the nominal flying condition as stable and large chaotic slider oscillations as unstable.

1. Touchdown – Takeoff Simulations

The topography of a disk is composed of harmonic and non-harmonic content at all wavelengths or frequencies as the disk spins. Figure 18 shows the experimentally measured frequency spectral contents of two disk's morphology as seen by the slider as the disk spins. Both disks are "super-smooth" media, however, it is seen that disk A is smoother than disk B across the entire spectral band. Figure 19 shows a TD – TO numerical simulation that is similar to that shown in Fig. 15, however the system is now forced with the measured disk topography from disk A. It is found that while decreasing FH_{ss} the slider "snaps" from stable motions about x_1^* into chaotic high amplitude oscillations. Upon increasing FH_{ss}, stable slider motion is resumed about x_1^*, exhibiting a FH hysteresis. Because this system exhibits *strange attractors* in the sub- 6 nm FH regime, the characteristics of the chaotic slider motion are highly dependent on the disk forcing. However, for all disk topographies investigated an unstable motion exhibiting a FH hysteresis was always present due to the intermolecular force. By qualitatively comparing the experimental result in Fig. 1b with the simulation results in Fig. 19 we see

that the maximum amplitude of vibration does not occur at the lowest FH_{ss}, but rather it occurs after the minimum FH_{ss} has been reached and increases with increasing FH_{ss}.

2. Transition between stable and unstable flying

Experimentally it was shown that by changing the FH only slightly the transition between stable and intermittent unstable flying was abrupt (see Fig. 1a). Numerical simulations have also been carried out showing this phenomenon in which the FH_{ss} is held fixed. Within the regime where the system exhibits a double-well potential, it has been shown that the slider can be easily forced into unstable high amplitude oscillations. Figure 20 shows the slider motion exhibiting intermittent instability at FH_{ss} = 3.35 nm. Figure 21 shows a similar simulation without including the intermolecular force. These two figures show that the intermittent instability here is due to the inclusion of the intermolecular force. By slightly increasing the FH_{ss}, the instability ceases to exist and by slightly decreasing the FH_{ss}, the instability will persist indefinitely. Under these conditions, the slider has the ability to oscillate about x_3^*, x_1^*, or both x_3^* and x_1^* and can switch between oscillation states chaotically. Figure 22 presents a plot of the state-space showing oscillations about x_3^*, x_1^*, and both x_3^* and x_1^*. Figure 23 shows the chaotic nature of the system as it switches between oscillation states. It is seen that when the system becomes unstable, the most likely oscillation state of the slider is oscillation about both x_3^* and x_1^*. It is possible for the slider to oscillate about x_3^* but due to the disk forcing, the slider cannot continue oscillating about this equilibria. If a slider could remain in the state of oscillation about x_3^*, a stable sub- 1 nm FH slider could be realized. However, due to disk waviness, roughness and glide-height, the result is high amplitude unstable oscillations.

PARAMETRIC STUDY

The above 1DOF system used to simulate the HDI is greatly simplified to give an understanding of the effects of adding intermolecular forces in the system and to show how certain parameters affect HDI dynamic stability. However, due to the assumptions made in reducing the HDI to a 1DOF system, the results must be viewed as merely qualitative. It is desired to make the HDI as stable as possible, and thus far it has been shown that stability can be highly compromised when flying in the sub– 6 nm regime due to the presence of intermolecular forces. Nominal values have been used in the simulations presented. Next we present some qualitative results on how these parameters affect the HDI stability as they are varied.

It was shown that the slider has the ability to become unstable when multiple equilibria exist. Therefore, if it were possible to exclude this regime of multiple equilibria, the slider system dynamics would be much simplified, and not exhibit instability and a FH hysteresis due to intermolecular forces. However, the inclusion of the intermolecular forces in the modeling will always predict this regime. The bifurcation plot in Fig. 14 is useful in visualizing the regime where multiple equilibria exist, and the model elements controlling the location and length of this regime are both the intermolecular and the air bearing forces.

(a) Intermolecular Force

The cause of the complicated dynamics of this system stems from the intermolecular force. By simply scaling the intermolecular force in Eq. (4) as shown in Fig. 24, we obtain the corresponding bifurcation plots as shown in Fig. 25, which clearly

illustrates its effect on HDI stability. It is seen that by decreasing the intermolecular force to one-fourth and one-half its nominal value, the multiple equilibria regime shrinks from $1.35 < FH_{ss} < 6.3$ nm to $0.9 < FH_{ss} < 1.8$ nm and $1.1 < FH_{ss} < 3.3$ nm, respectively. These decreases result in much smaller FH regimes where the system has the ability to become unstable. On the other hand, by increasing the intermolecular force by two times its nominal value, the multiple equilibria regime increases to $1.65 < FH_{ss} < 12.3$ nm. Figure 26 presents plots of the slider's motion flying over a measured disk topography at a FH_{ss} of 3 nm for different amplitudes of the intermolecular force. It is seen that as the intermolecular force increases, so does the instability of the HDI. Figure 27 shows the TD – TO FH hysteresis simulation results as a function of intermolecular force amplitude. It is seen that as the intermolecular force is increases, so does the FH hysteresis.

Even though the intermolecular force cannot be attenuated completely, there are ways to reduce its effect. Decreasing the effective slider area within proximity of the disk is the most effective method (recall Eq. (1)). This reduction in area can come from texturing the ABS, through design of the ABS rails, form-factor (nano, pico, femto, etc.) and by slider attitude. Figure 28 shows the intermolecular force as a function of minimum spacing for different pitch angles and form-factors for two different ABS designs. It is seen that the larger the rear ABS rail within proximity of the disk surface, the higher the adhesion force. Also, other factors such as crown, camber and twist will substantially affect the adhesion force. By simply decreasing the rear ABS pads area, the adhesion force decreases, however, for manufacturability, flyability, stability, and other design criteria, the rear ABS pad has to have certain minimum dimensions. Also, the intermolecular force scales proportionally with the Hamaker constant. In this analysis, a

nominal value of $A = 10^{-19}$ J was used, however, this value is only approximate. A more accurate value of the Hamaker constant needs to be obtained for the HDI. Also, surface chemistry could also change the Hamaker constant between various lubricants and DLC coatings. Some recently published values of the HDI Hamaker constant are $A = 0.724\times10^{-19}$ J with lubricant on the disk surface and $A = 1.80\times10^{-19}$ J without lubricant at the interface [11]. These values are close to what has been used in this analysis; therefore it is expected that the adhesion force will always be present below 3.5 nm FH's causing possible HDI instabilities.

(b) Air Bearing Stiffness: nonlinear

The air bearing stiffness is another variable affecting the nature of multiple equilibria. The air bearing stiffness is a function of the ABS design, suspension pre-load, slider attitude, relative disk velocity, and other design parameters. Generally, the linearized "vertical" resonant mode of vibration of an air bearing – slider system is between 150 kHz and 400 kHz. For large oscillations, the slider exhibits a power hardening stiffness as modeled in Eq. (2). A change in the stiffness by factors in the range of 0.25 – 4 changes the linearized resonant frequency half to twice the nominal value: 108.6 – 434.4 kHz. The bifurcation plots associated with the factors 0.25 and 4 are shown in Fig. 29. A series of simulations was performed at a FH_{ss} of 3 nm showing how the stiffness affects the HDI stability. It is seen from the results shown in Fig. 30 that stability increases as the air bearing stiffness increases. Also, the TD – TO FH hysteresis was simulated as a function of air bearing stiffness, and the results are shown in Fig. 31. The trend between the FH hysteresis and air bearing stiffness does not appear to be monotonic. This is due to the complex disk forcing function and the varying air bearing

resonant frequency as the stiffness changes. The disk topography frequency spectra is not uniform across the frequency band, and at different resonant frequencies, the disk affects resonance differently. However, there is an overall decreasing trend of the FH hysteresis as the stiffness is increased.

(c) Air bearing Stiffness: linear

If the air bearing stiffness were linear and not a power-hardening nonlinear spring as described in Eq. (2), the bifurcation plot would be affected as would be the stability. In Fig. 32 the bifurcation plots are shown for linear stiffnesses of $k_o = 3\times10^6$ N/m, $k = k_o*2$, and $k = k_o*4$. In comparing these results with those for a nonlinear air bearing stiffness in Fig. 29 we see that the FH regime where all three equilibria exist (unstable regime) is larger for the linear stiffness cases. By increasing the extent of the unstable regime, we know that the stability of the HDI would be less. We conclude that the power-stiffening air film of an actual air bearing is extremely beneficial in increasing the stability of the HDI.

(d) Air bearing damping

As with the air bearing stiffness, air bearing damping is also a function of many parameters. Generally, the linearized "vertical" mode damping is between 1 % to 5 % of critical damping. In the previous two sections the bifurcation plots were used to show the degree of instability. On the other hand, air bearing damping does not change the bifurcation plots. In nonlinear systems, generally, more damping enhances stability. Indeed we find similar results here. Figure 33 presents the effect of damping on slider

instability at a FH_{ss} of 3.4 nm as the damping is varied from 0.46 to 3.64 %. It clearly shows that the higher the damping, the more stable the HDI becomes. Also, the dependence of the FH hysteresis on damping as determined by TD – TO simulations is summarized in Fig. 34, which shows that the FH hysteresis decreases as the damping is increased.

(e) Disk topography

As seen in Fig. 18, disk topographies can vary substantially depending on substrate material, texturing, and other process conditions. The forcing and initial conditions of nonlinear systems of the type described here are the most sensitive variables to their chaotic nature that leads to the unstable oscillations. When the HDI model exhibits a double-well potential chaotic oscillations can arise even when it is forced by a single harmonic excitation. Figure 35 shows a plot of single frequency disk forcing amplitude, A_d, where the slider steady-state motion becomes unstable versus disk forcing frequency, f_d, where $d(t) = A_d \sin(2\pi f_d)$ at initial conditions of *(FH , velocity) = (3.4 nm , 0 mm/s)* at a FH_{ss} =3.4 nm. Above the curve shown in Fig. 35, the slider's response is unstable and below it, the response in stable for a single frequency excitation. It is observed that the most sensitive forcing frequency is around the systems linearized resonant frequency of approximately 175 kHz. Unfortunately a technique such as superposition cannot be used to extend the results in Fig. 35 to the complicated disk forcing by an actual disk. Figure 36 compares the TD – TO FH hysteresis simulation results for the two disks A and B described in Fig. 18. It is observed that as the FH_{ss} transitions from 12.65 – 4.65 – 12.65 nm, disk B forces the HDI to transition into unstable slider oscillations while the forcing of disk A is too small at these FH_{ss} to

transition the slider into unstable oscillations. This result suggests that wavier and rougher disks result in HDI instability at much higher FH_{ss} values. By just varying the amplitude of disk A, another parametric study is performed, and the results are presented in Fig. 37, which shows the TD – TO FH hysteresis simulations for amplitude multiples of 0.25 to 4 times its original topography. It is observed that as the disk topography amplitude is increased, the FH hysteresis remains relatively constant at $DFH \approx 1$ nm, but the unstable response amplitude increases.

DISCUSSION

Experimental evidence of low FH slider instabilities is evident from two effects: (1) the "snapping" effect from stable to intermittently unstable and further to indefinitely unstable proximity and, (2) the presence of the FH hysteresis. Adhesion forces due to capillary (meniscus) effects appear to unlikely be the cause of these instabilities due the short time duration the slider is in contact with the lubricant film. Also, the experimental FH hysteresis results showed no dependence on lubricant thickness, for the thickness range tested. On the other hand, the time independent intermolecular adhesion force was shown to be significant when a slider and disk come within proximity of each other. The Lennard-Jones model was used to incorporate additional adhesion and repulsion forces into the CML Static Air Bearing Simulation Code solutions and into a simple lumped parameter 1DOF model. The 1DOF model was used for investigating the experimentally observed nonlinear dynamics associated with the HDI. It was shown from bifurcation plots of the system, that as the FH approaches sub– 6 nm, multiple equilibria exist. Also, for lower FH, the intermolecular force overcomes the air bearing load capacity and the

slider "snaps" down onto the disk. From a static analysis, one would expect that the only effect caused by intermolecular forces are at low FH's would be a static spacing loss, and by further decreasing the FH, the intermolecular forces would overcome the air bearing load capacity (Fig. 10b). However, a much greater implication arises when including the intermolecular force that has not been previously addressed – that of dynamic instability. It was shown that the possibility of the HDI becoming dynamically unstable is restricted to a regime where multiple equilibria exist, which extends into FH's much higher than those resulting from static analysis. The dynamics associated with a double-well potential system can be quite complicated when the system is forced, as was shown. The chaotic characteristic of the system with a double-well potential is what causes the HDI instability due to intermolecular forces. By numerically investigating both constant FH and the hysteresis TD – TO process, we were able to reproduce the experimental findings of HDI instability and FH hysteresis. Also, several qualitative features demonstrated by the experimental and simulation results are in agreement, including the effect of adding small DLC pads to decrease the sliders instability vibrations (decreases adhesion forces) and the asymmetric slider vibration amplitude during the TD – TO process.

These results imply that the HDI has a fundamental lower limit of FH at which the slider remains stable. This lower limit is a function of not only the disk morphology but also the ABS design and slider attitude. For the nominal values studied here, it was shown that the slider transitions into unstable oscillations at a FH_{ss} of 3 nm and 4.6 nm while flying over two different disks, A and B, respectively. It was shown by a parametric study that the FH at which instability occurs as well as the severity of the oscillations change with the parameters. The effect of the parameters discussed must be

understood to obtain a stable HDI design when flying extremely low. Also, it was shown that the power-stiffening feature of an air bearing increases the HDI stability. In order of importance, we found that the following parameters can be adjusted to obtain maximum HDI stability: (1) the intermolecular force should be reduced, (2) the disk morphology and slider should be optimized to produce minimum FHM, (3) air bearing stiffness should be increased, and (4) air bearing damping should be increased. It was shown for all the parameter values studied, HDI stability can always be compromised, however, by considering the findings in this paper, the instability due to intermolecular forces can be minimized.

The analysis presented here is based on adhesion modeled by the Lennard-Jones potential. The functional form of the repulsion term in Eq. (4) stems from the need for a repulsion term as the two mating surfaces contact one another. This approach lacks physical basis due to the fact that the two surfaces never actually come into contact. A more physical and complicated approach would be to model the repulsion as a contact force, similar to what was done in the Derjaguin-Muller-Toporov (DMT) model and the extension that Cheng, Etsion and Bogy (CEB) made [19] - [21]. In the DMT and CEB models, the attractive force is similar to Eq. (4) but the repulsion force stems from physical contact as seen in Fig. 38. For a simple spherical asperity impinging on a flat surface the forces generated as a function of separation distance are [19], [20]

$$F_{vdW}(x) = -\frac{AR}{6x^2} \qquad \text{for } x > a_o$$

$$F_{DMT}(x) = -\frac{AR}{6x^2} + \frac{4}{3}E^*\sqrt{R}(a_o - x)^{3/2} \qquad \text{for } x \le a_o \tag{11}$$

where R is the radius of the spherical asperity, E^* is the effective elastic modulus, and a_o is the intermolecular distance usually taken to be about two angstroms. However, by comparing the additional force that is generated by Eq. (4) (see Fig. 24) and by the DMT and CEB models, we find that similar force curves are generated. Therefore, by using either the simplistic approach of the analysis in this paper in modeling the repulsion by Eq. (4) or by including a complex contact force from the CEB model, we would expect to find qualitatively similar dynamic instability results.

Another simplification of the modeling here was to neglect surface roughness effects. It can be seen from Eq. (1) that the adhesion force scales proportionally with the area within proximity. Due to the qualitative nature of the 1DOF HDI model, the roughness effect can be discussed only qualitatively. By including the surface roughness of the slider and disk, we would expect the adhesion force to be effectively decreased. This effect is covered in the parametric study of scaling the intermolecular force. Increasing roughness decreases the intermolecular force, hence, leads to an increase in HDI stability. However, in order to achieve a non-contact 3.5 nm FH HDI, the slider and disk surfaces must be extremely smooth.

CONCLUSION

Experimentally it is observed that as a slider flies within proximity of the disk HDI dynamic stability is lost. Additional forces due to capillary and intermolecular adhesion were considered. Due to the kinetic formation of a meniscus and the experimental results presented, we concluded that meniscus forces need not be considered in the dynamic modeling of the HDI. A nonlinear dynamic analysis of a modeled HDI incorporating intermolecular forces revealed a new kind of dynamics that

cannot be captured by static analysis. By analyzing the systems equilibria and stability, it was found that multiple equilibria exist in the sub – 6 nm FH regime associated with a double-well potential. Within this regime the sliders motion can be stable or chaotically unstable when it is externally forced by a disk topography. From the analytical and numerical analysis presented here, the experimentally measured FH hysteresis, the intermittent slider instability and the abrupt transition between stable and unstable proximity can be explained. A parametric study was used to show how the variables affect HDI stability. Also, the effect of the power-hardening air bearing stiffness was shown to be beneficial in increasing HDI stability. By optimizing the parameters such as the air bearing design and the disk morphology, the stability of the HDI can be improved. However, for practical values of the parameters, it is found that instability is likely to occur when flying below 6 nm. From these results, we are forced to conclude that there maybe a fundamental lower FH limit for a give slider – disk combination, below which the slider would not be able to fly due to HDI dynamic instability caused by intermolecular adhesion forces.

ACKNOWLEDGEMENTS

We would like to thank Rocky Mai for aiding in some of the experiments. This work was supported by The Computer Mechanics Laboratory at the University of California, Berkeley, USA and the Information Storage Industry Consortium (INSIC).

REFERENCES

[1] R. Wood, “The feasibility of magnetic recording at 1 terabit per square inch,” *IEEE Trans. Magn.*, vol. 36, pp. 36-42, Jan. 2000.

[2] B. H. Thornton, and D. B. Bogy, "Non-Linear Aspects of Air Bearing Modeling and Dynamic Spacing Modulation in Sub 5 nm Air Bearings for Hard Disk Drives," presented at TMRC 2002, to be published, *IEEE Trans. Magn*

[3] X. Ma, D. Kuo, J. Chen, H. Tang, and J. Gui, "Effect of lubricant on flyability and read-write performance in the ultra-low flying regime," *Proceedings of the Symposium on Interface Tribology Toward 100 Gb/in^2*, C. S. Bhatia, A. A. Polycarpou, and A. Menon, eds., ASME Trib-Vol. 10, Seattle, WA, pp. 27-34, Oct. 2000.

[4] T. Kato, S. Watanabe, and H. Matsuoka, "Dynamic characteristics of an in-contact headslider considering meniscus force: part 1—formulation and application to the disk with sinusoidal undulation," *ASME J. of Tribology*, vol. 122, pp. 633-638, July 2000.

[5] T. Kato, S. Watanabe, and H. Matsuoka, "dynamic characteristics of an in-contact headslider considering meniscus force: Part 2 – application to the disk with random undulation and design conditions**,"** *ASME J. of Tribology*, vol. 123, pp. 168-174, Jan. 2001.

[6] T. Kato, S. Watanabe, and H. Matsuoka, "dynamic characteristics of an in-contact headslider considering meniscus force: Part 3 – formulation and application to the disk with sinusoidal undulation," *ASME J. of Tribology*, vol. 124, pp. 801-810, Oct. 2002.

[7] C. Gao, and B. Bhushan, "Tribological performance of magnetic thin-film glass disks: its relation to surface roughness and lubricant structure and its thickness," *Wear*, vol. 90, pp. 60-75, 1995.

[8] Autumn, K., M. Sitti, A.M. Peattie, W. Hansen. S. Sponberg, Y.A. Liang, T. Kenny, R. Fearing, J.N. Israelachvili, R.J. Full, "Evidence for van der Waals adhesion in gecko setae," PNAS, vol. 99(19): 12252-12256, 2002.

[9] L. Wu, and D. B. Bogy, "Effect of the intermolecular forces on the flying attitude of sub- 5 nm flying height air bearing sliders in hard disk drives," *ASME J. of Tribology*, vol. 124, pp. 562-567, July, 2002.

[10] J. H. Li, B. Liu, W. Hua, and Y. S. Ma, "Effects of intermolecular forces on deep sub- 10 nm spaced sliders," *IEEE Trans. Magn* , vol. 38, pp. 2141-2143, Sept. 2002.

[11] B. Zhang, and A. Nakajima, "Possibility of surface force effect in slider air bearings of 100 Gbit/in^2 hard disks," *Tribology International*, vol. 36, pp. 291-296, 2003.

[12] R.H. Wang, V. Raman, U.V. Nayak, "Head-Disk Interface Issues for Near Contact Recording," *Proceedings of the Symposium on Nanotribology and Nanotechnology*

for 1 Tbit/in^2, A. A. Polycarpou, and C. Singh Bhatia, eds., ASME Trib-Vol. 11, San Francisco, CA pp. 37-43, 2001.

[13] N.V. Gitis, L. Volpe, "Nature of static friction time dependence," *J. Phys. D: Appl. Phys.*, Vol. 25, pp. 605-612, 1992.

[14] J. N. Israelachvili, *Intermolecular and surface forces, 2nd ed.* San Deigo: Academic Press, 1992.

[15] S. H. Strogatz, *Nonlinear Dynamics and Chaos*. Cambridge: Perseus Books, 1994.

[16] L. N. Virgin, *Introduction to Experimental Nonlinear Dynamics: A case study in mechanical vibration*. New York: Cambridge University Press, 2000.

[17] F. C. Moon, and P. J. Holmes, "Magnetoelastic strange attractor," *J. of Sound and Vibration*, vol. 65, pp. 275-296, 1979.

[18] P. J. Holmes, and F. C. Moon, "Strange attractors and chaos in non-linear mechanics," *ASME J. of Applied Mechanics*, vol. 50, pp. 1021-1032, 1983.

[19] B. V. Derjaguin, V. M. Muller, and Y. P. Toporov, "Effect of contact deformations on adhesion of particles," *J. of Colloid and Interface Sci.*, vol. 53, pp. 314-326, 1975.

[20] S. I. Lee, W. Howell, A. Raman, and R. Reiferberger, "Nonlinear dynamics of mircocantilevers in tapping mode atomic force microscopy: A comparison between theory and experiment," *Phys. Rev. B*, vol. 66, 115409, 2002.

[21] W. R. Chang, I. Etsion, and D. B. Bogy, "Adhesion Model for Metallic Rough Surfaces," *ASME J. of Tribology*, vol. 110, pp. 50-56, Jan. 1988.

Parameter	Nominal Value	Parameter	Nominal Value
b	244.1 [N/m]	B'	2.7×10^{-88} [N·m^9]
a	-0.48	m	1.6158×10^{-6} [kg]
A'	1.8×10^{-30} [N·m^3]	c	0.08 [N·s/m]

Table 1. Nominal values of constants used.

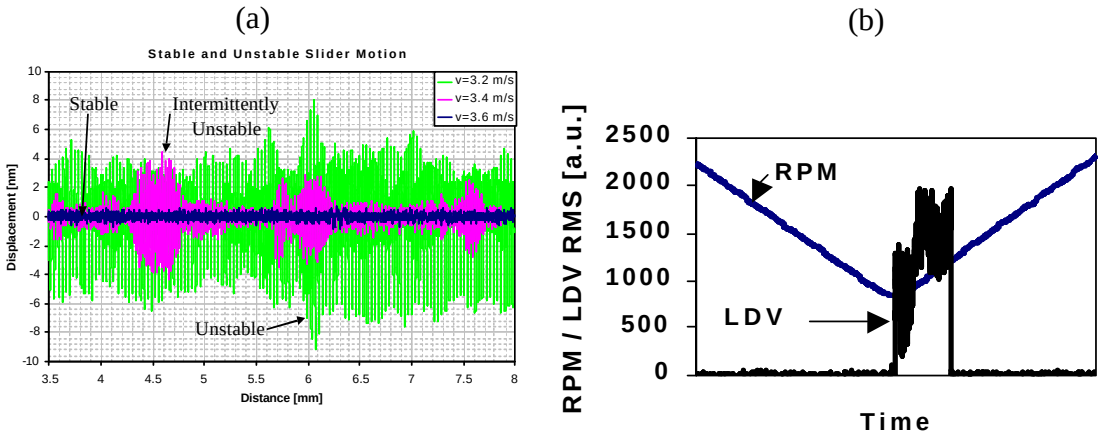

Fig. 1. (a) Time trace of the stable, intermittently unstable, and indefinitely unstable slider motion measured by LDV. (b) Measurement of the FH hysteresis as the FH is lowered and increased by changing the disk RPM.

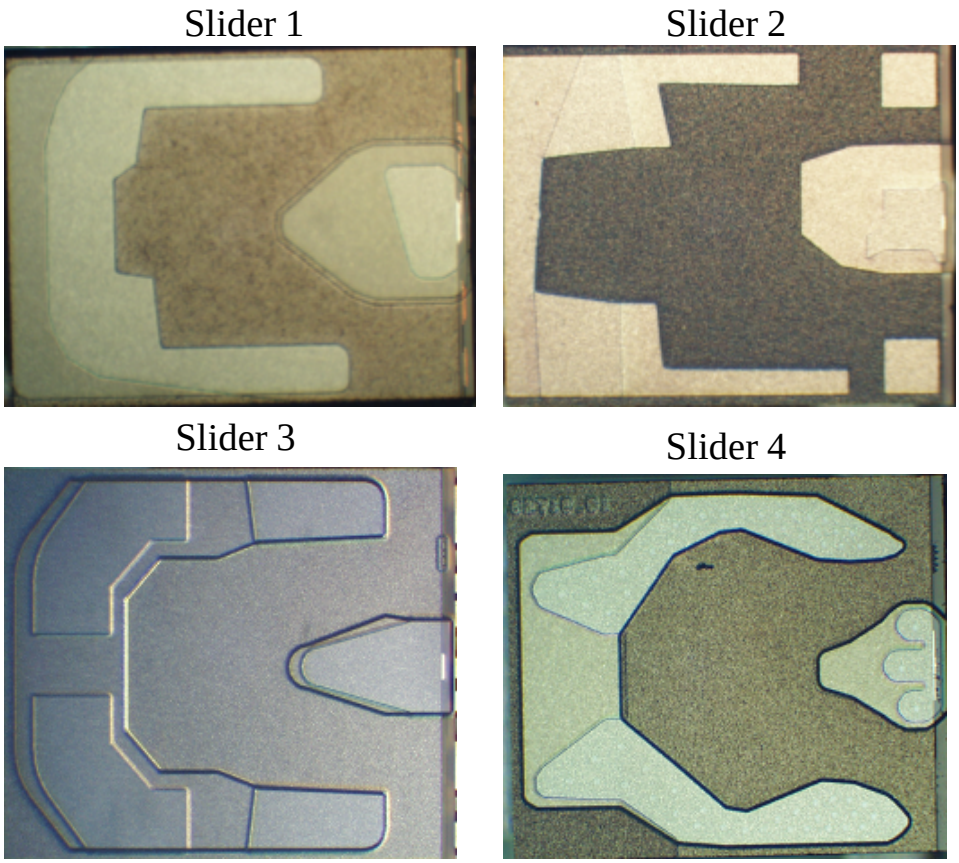

Fig. 2. Air bearing surface designs of four different pico size sub-ambient sliders.

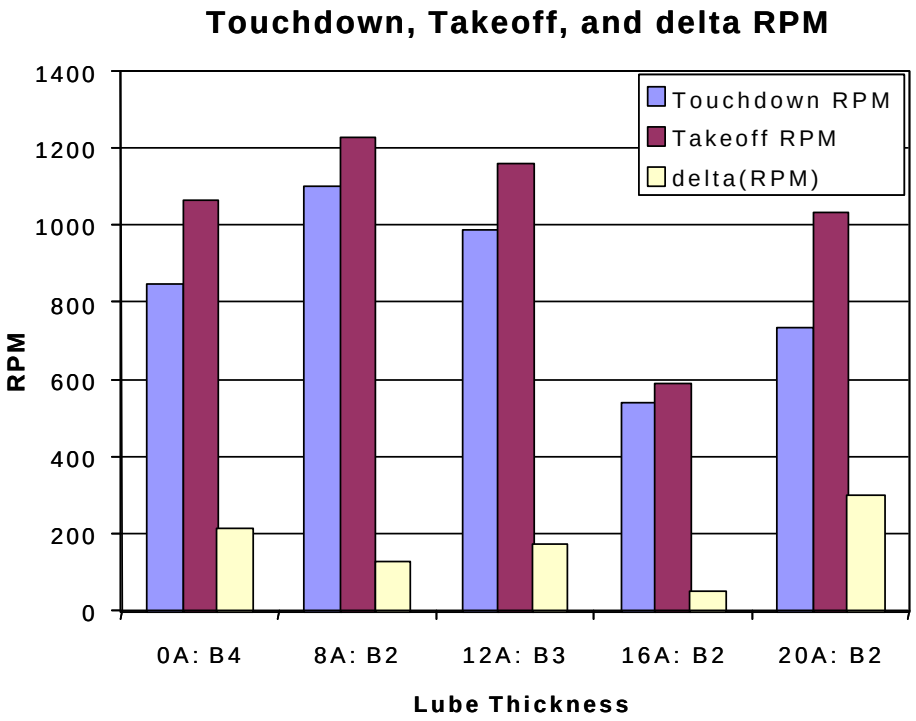

Fig. 3. Touchdown, takeoff, and FH hysteresis as a function of lubricant thickness for slider 1.

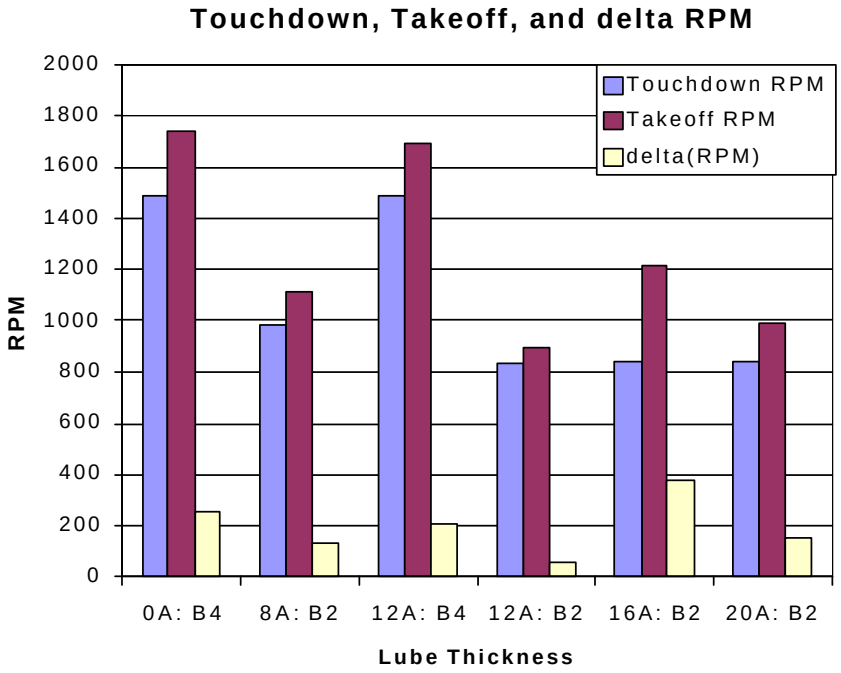

Fig. 4. Touchdown, takeoff, and FH hysteresis as a function of lubricant thickness for slider 2.

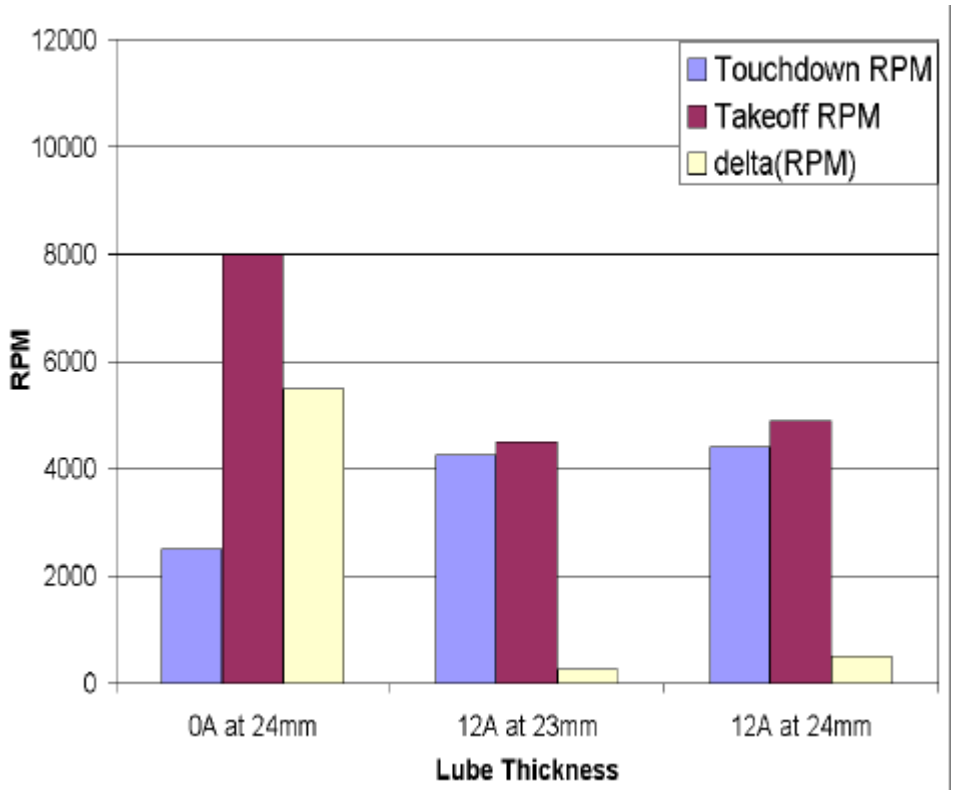

Fig. 5. Touchdown, takeoff, and FH hysteresis as a function of lubricant thickness for slider 3.

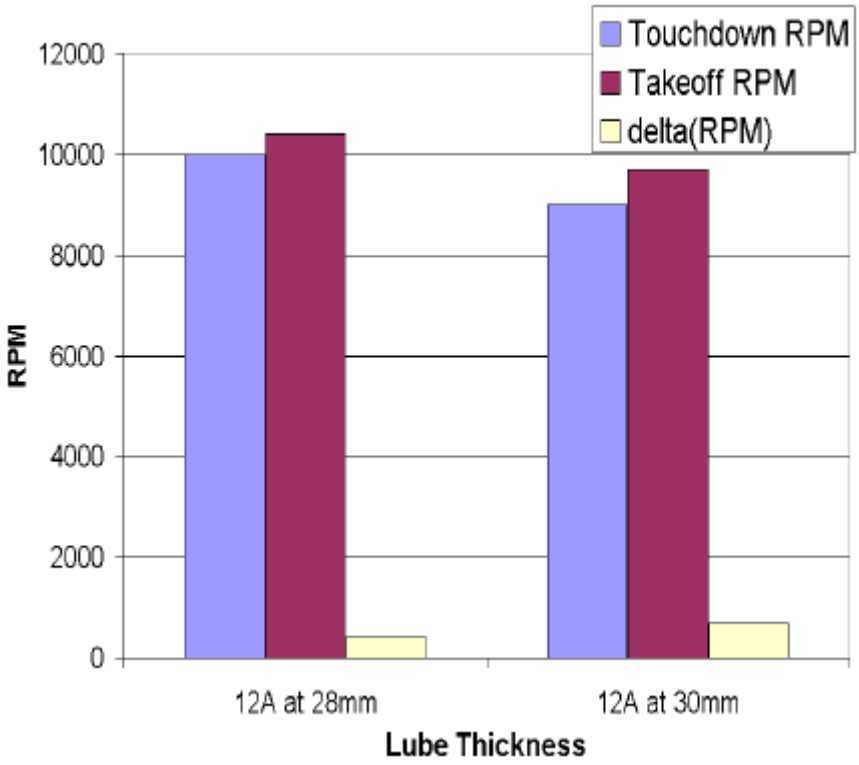

Fig. 6. Touchdown, takeoff, and FH hysteresis as a function of lubricant thickness for slider 4.

(a) (b)

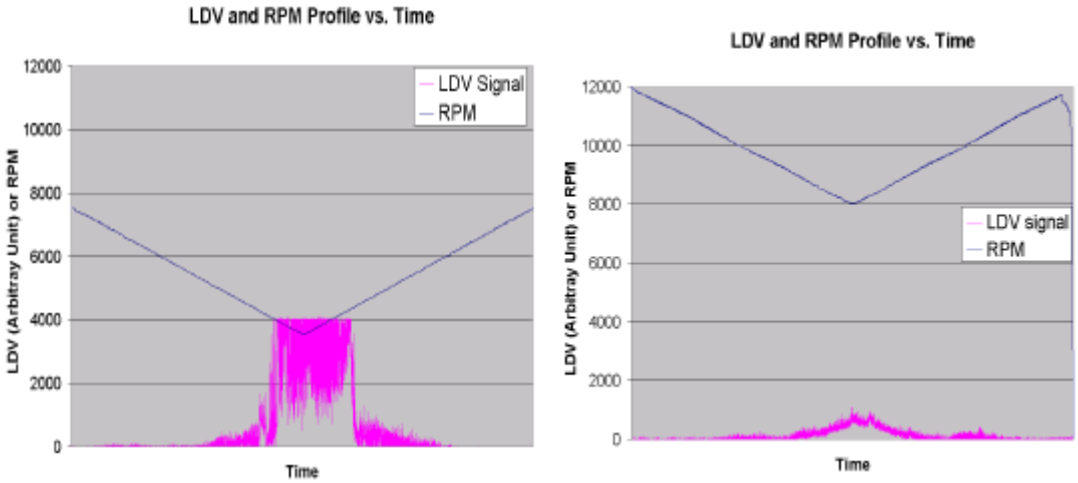

Fig. 7. Typical time traces of the RPM and LDV RMS for sliders (a) 1- 3 and slider (b) 4.

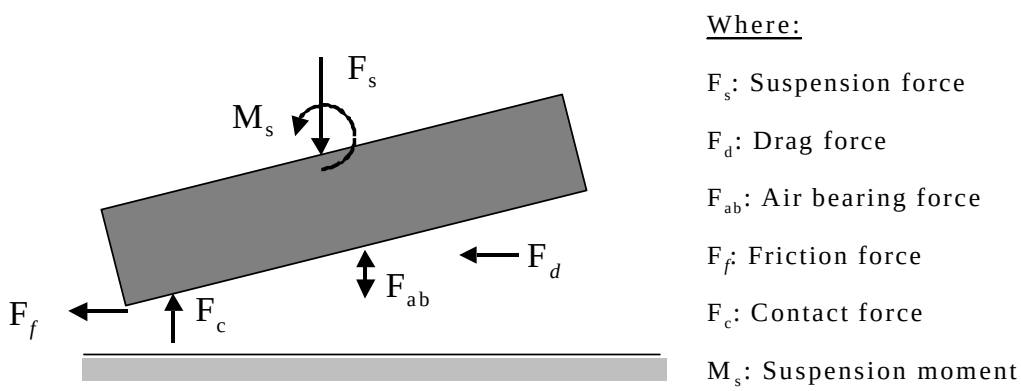

Fig. 8. Free-body diagram of the air bearing – slider model.

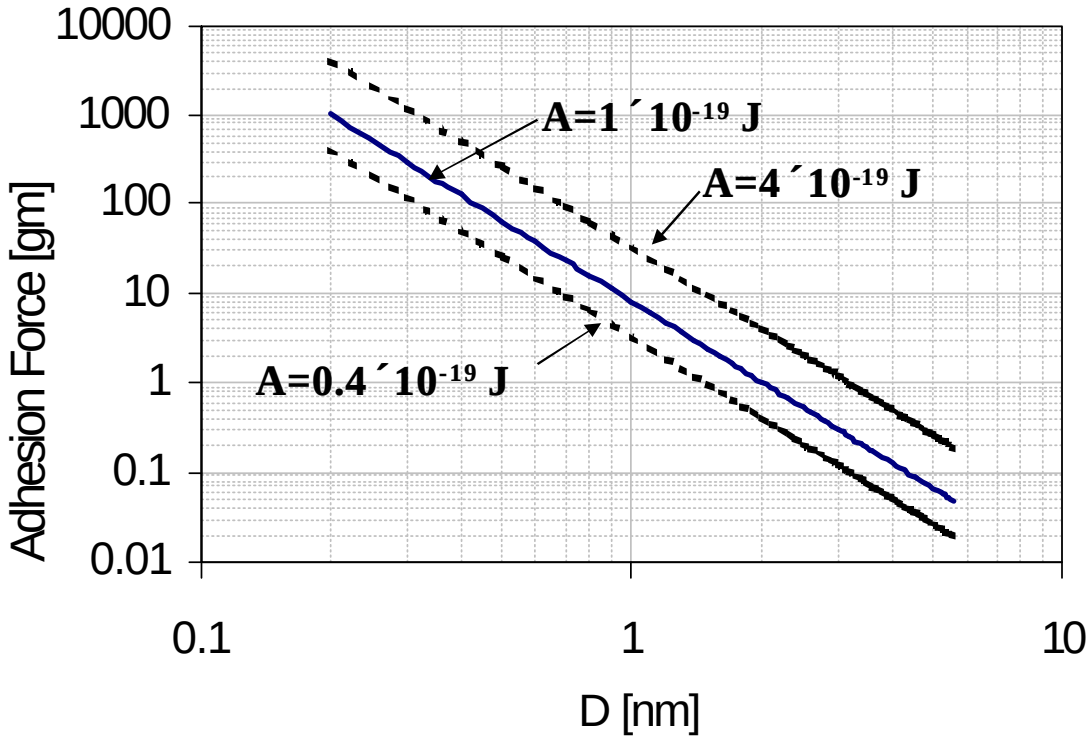

Fig. 9. Intermolecular adhesion force as a function of separation distance for two parallel flat surfaces.

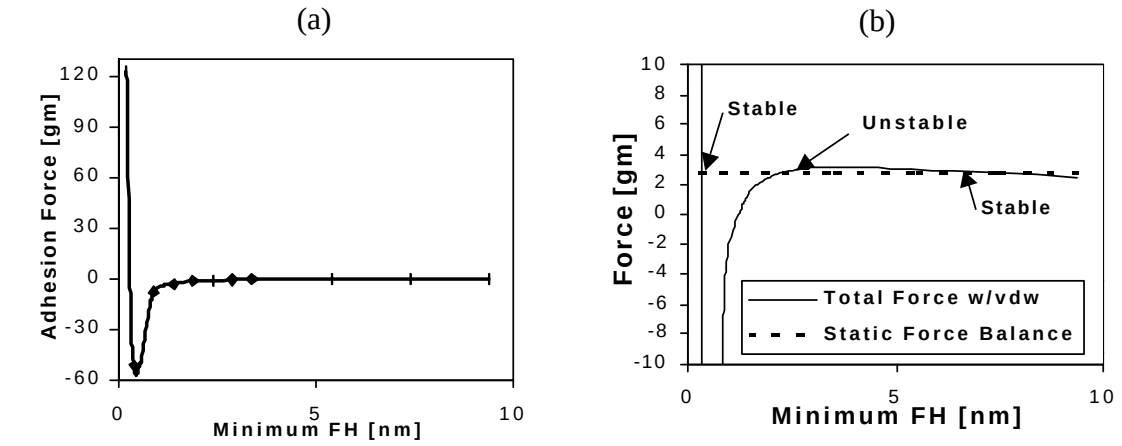

Fig. 10. (a) Intermolecular adhesion force modeled by the Lennard-Jones potential and (b) the resultant force acting on the air bearing as functions of the minimum FH.

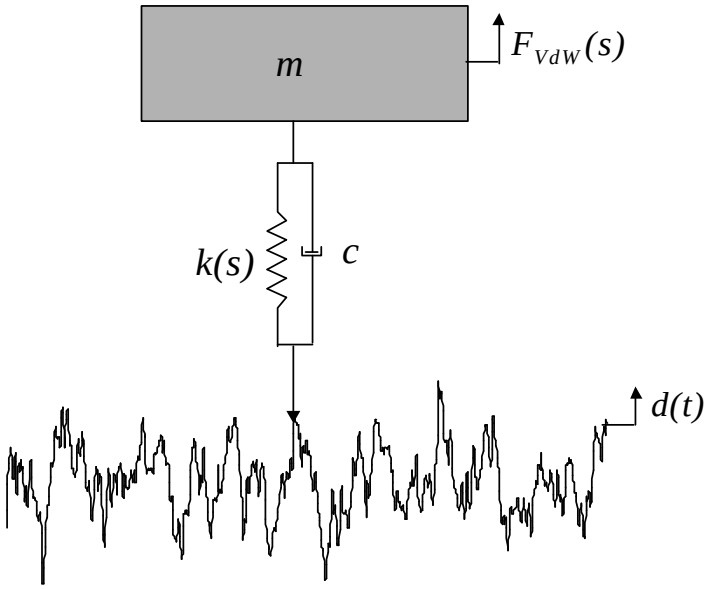

Fig. 11. Schematic of the 1DOF nonlinear model.

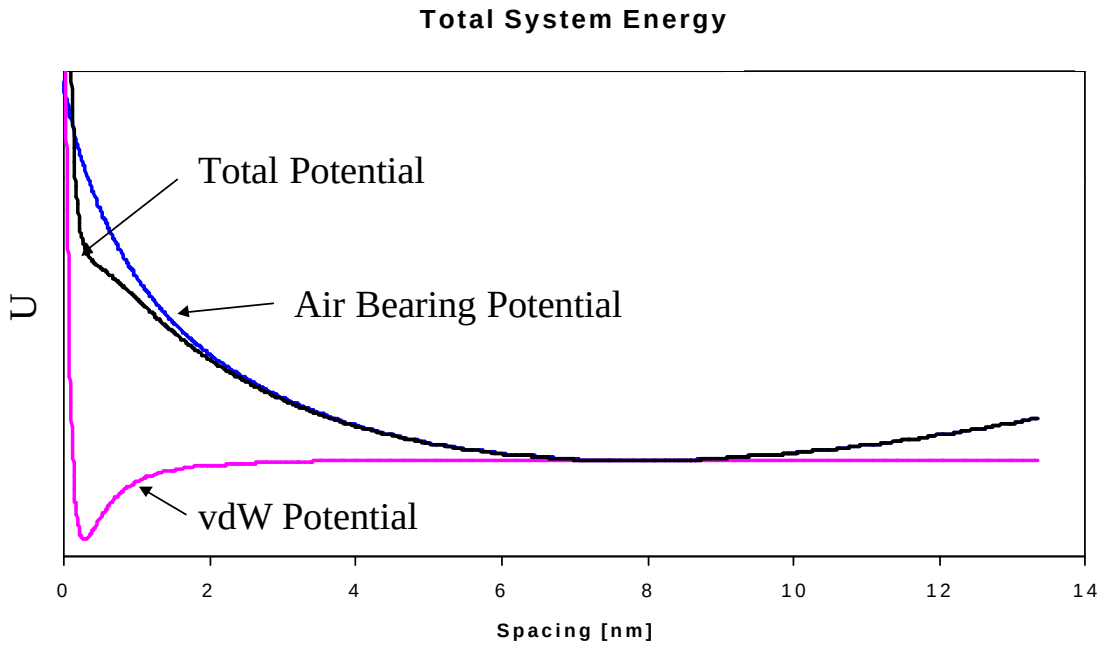

Fig. 12. Potential energy curves of the air bearing, Lennard-Jones and the total system at a FH_{ss} of 7.75 nm.

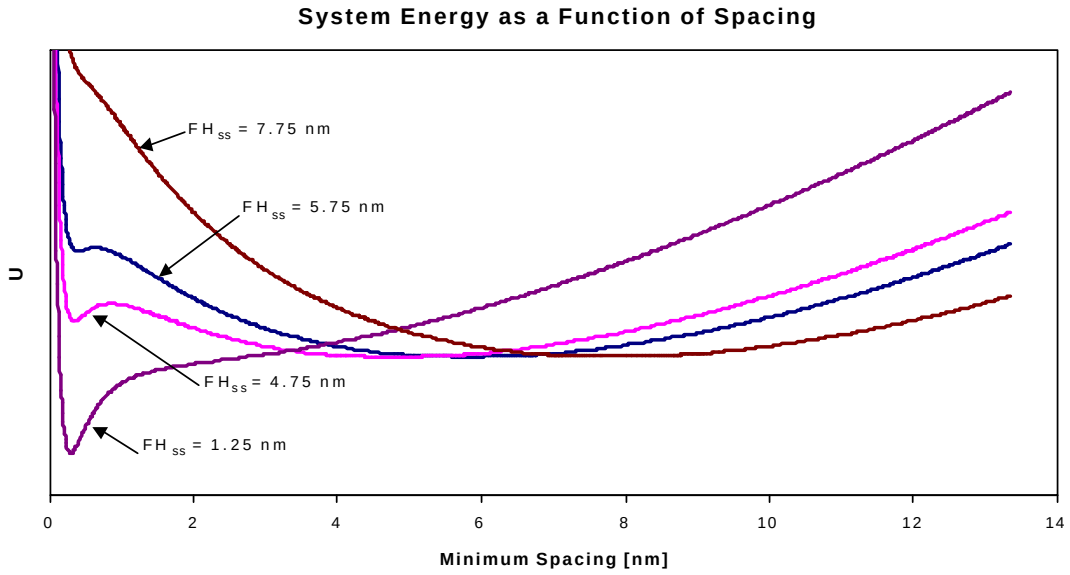

Fig. 13. Total system potential energy curves at a FH_{ss} of 7.75, 5.75, 4.75, and 1.25 nm.

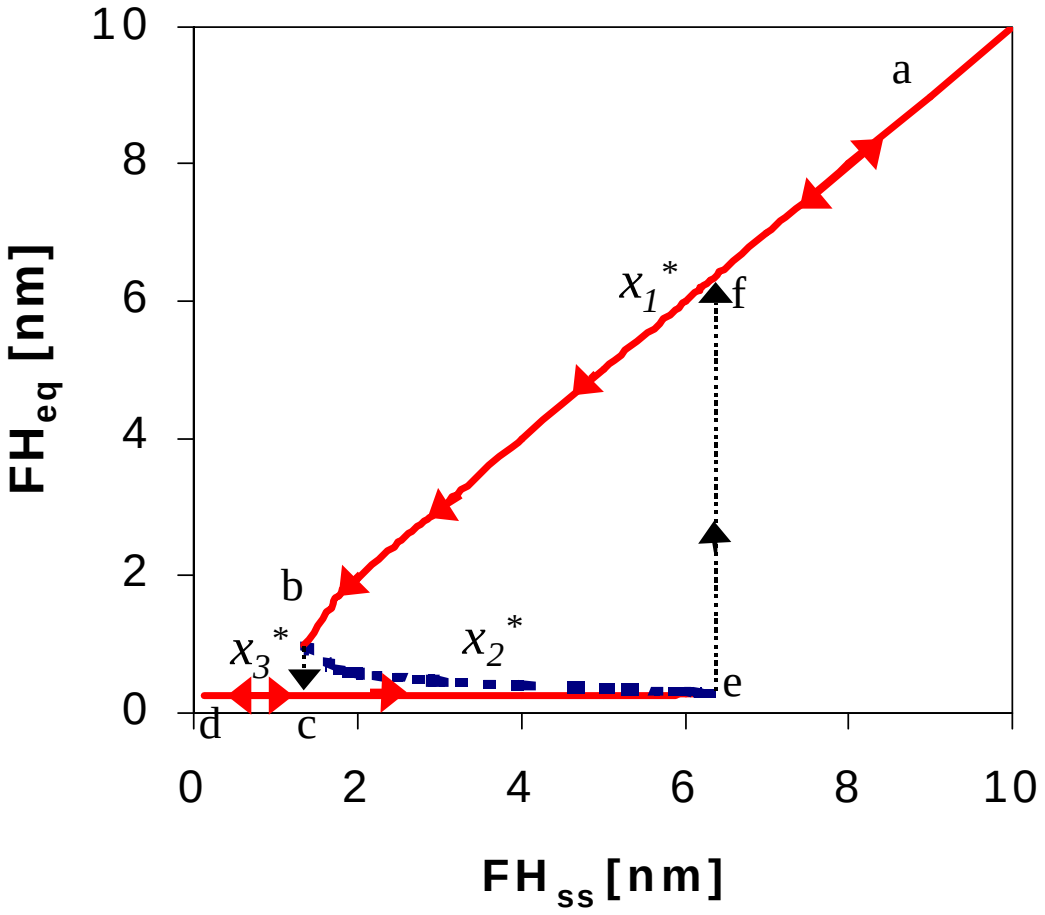

Fig. 14. Bifurcation plot showing FH_{eq} as a function of FH_{ss}. (–) stable, and (- -) unstable.

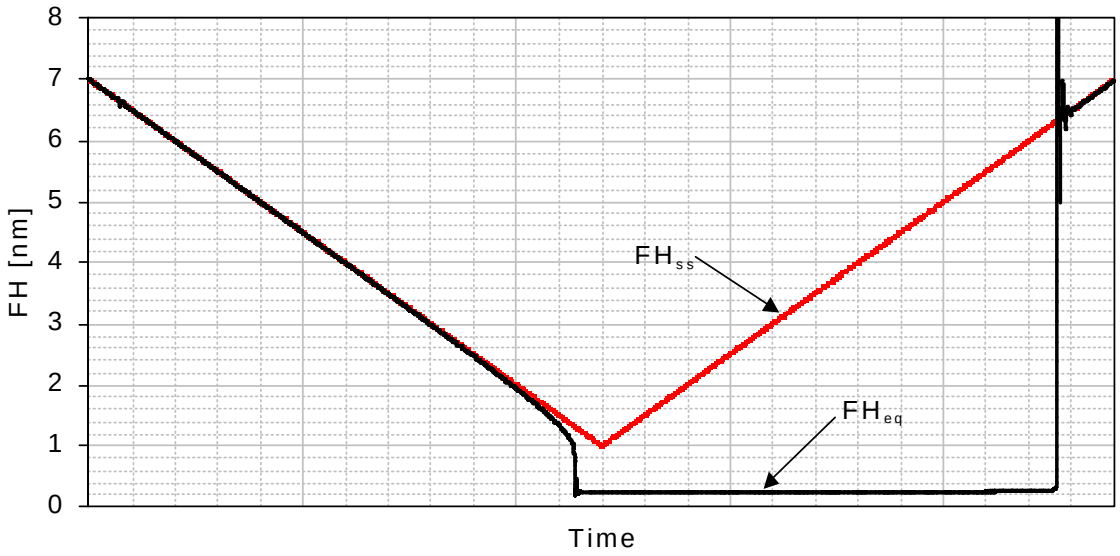

Fig. 15. Unforced TD – TO simulation showing the FH hysteresis is bound by the multiple equilibria regime.

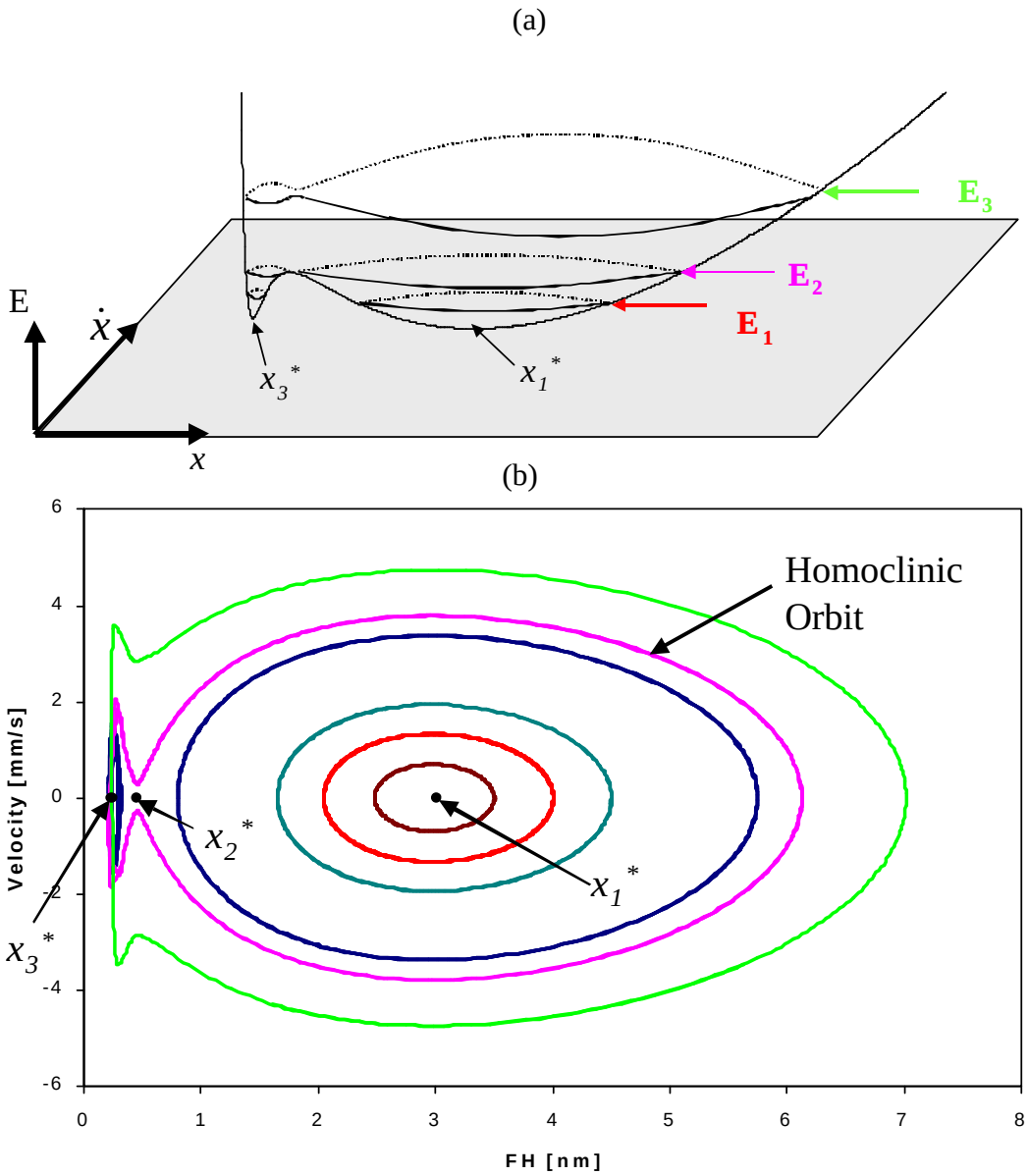

Fig. 16. (a) Sketch of the energy surface in state-space and (b) the trajectories projected onto the state-space plane for the unforced, undamped system.

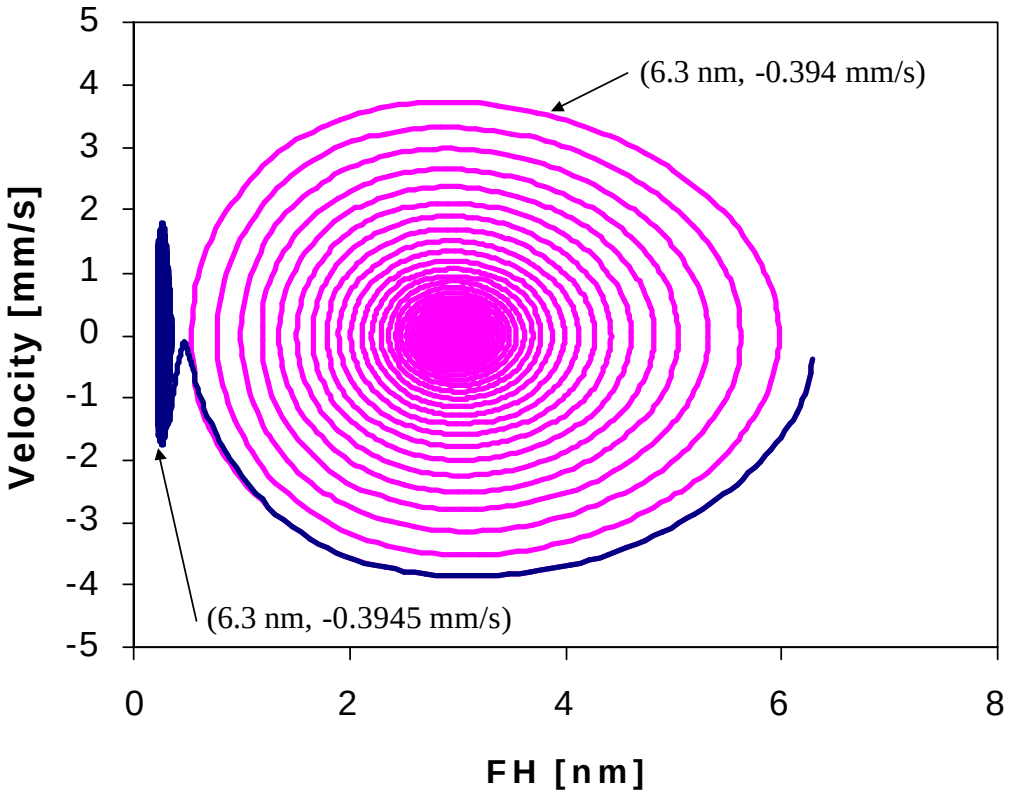

Fig. 17. State-space trajectories of the unforced system showing sensitivity to initial conditions.

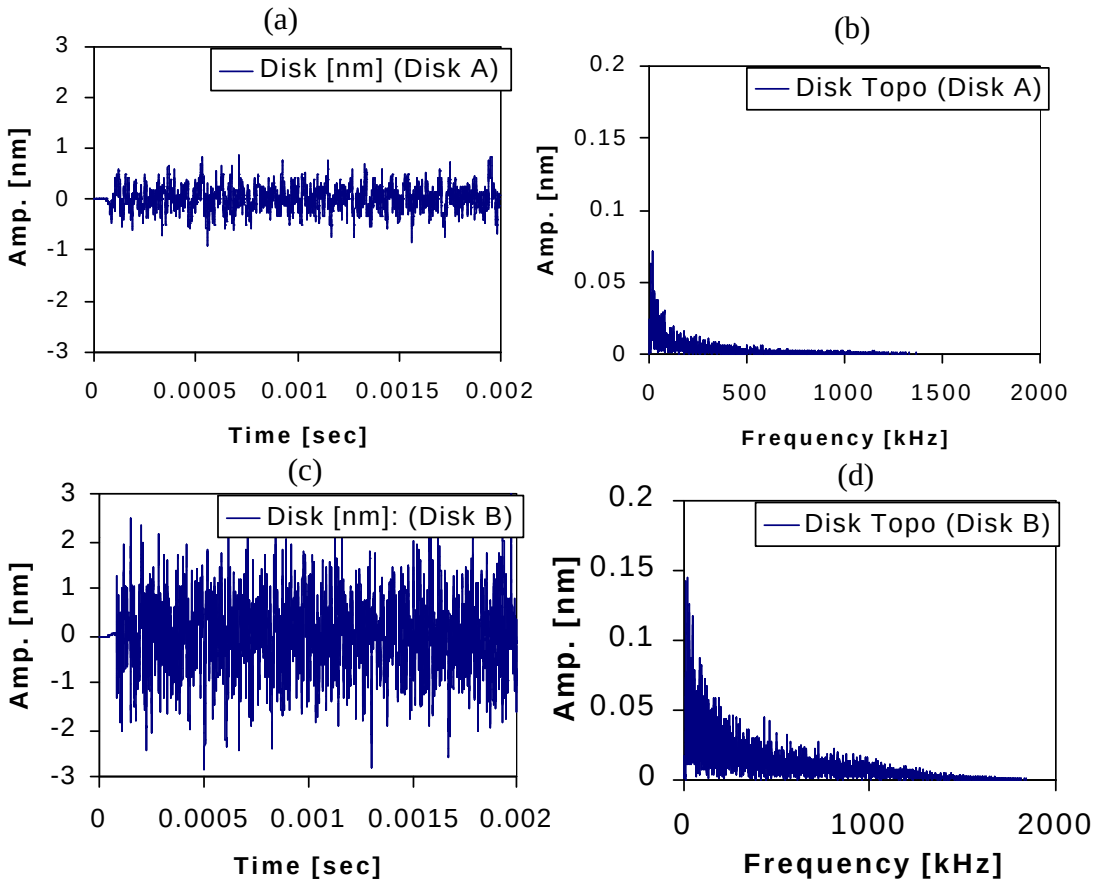

Fig. 18. (a) Topography of disk A and (b) its frequency content. (c) Topography of disk B and (d) its frequency content.

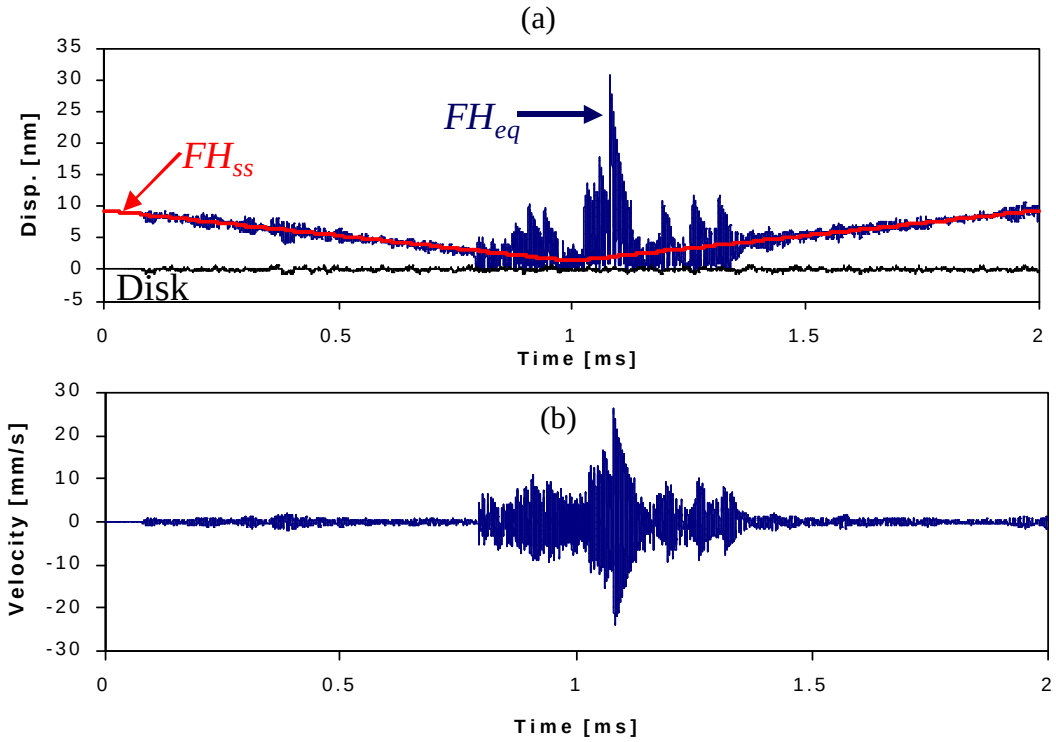

Fig. 19. Forced TD –TO simulation showing the (a) disk, FH_{ss} and FH_{eq} and (b) the sliders velocity as functions of time.

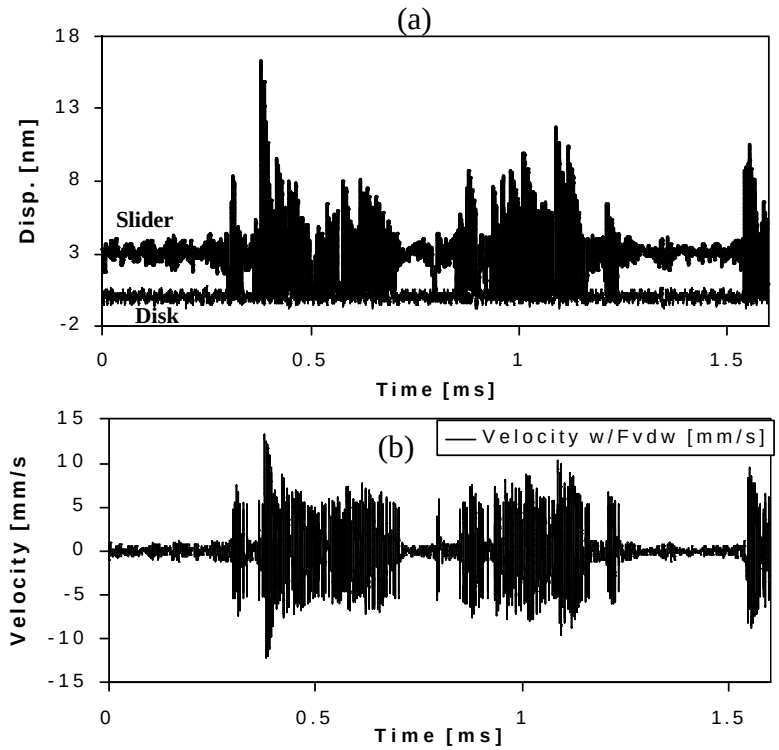

Fig. 20. Forced constant FH_{ss} simulation showing the (a) disk and sliders displacement and (b) the sliders velocity as functions of time.

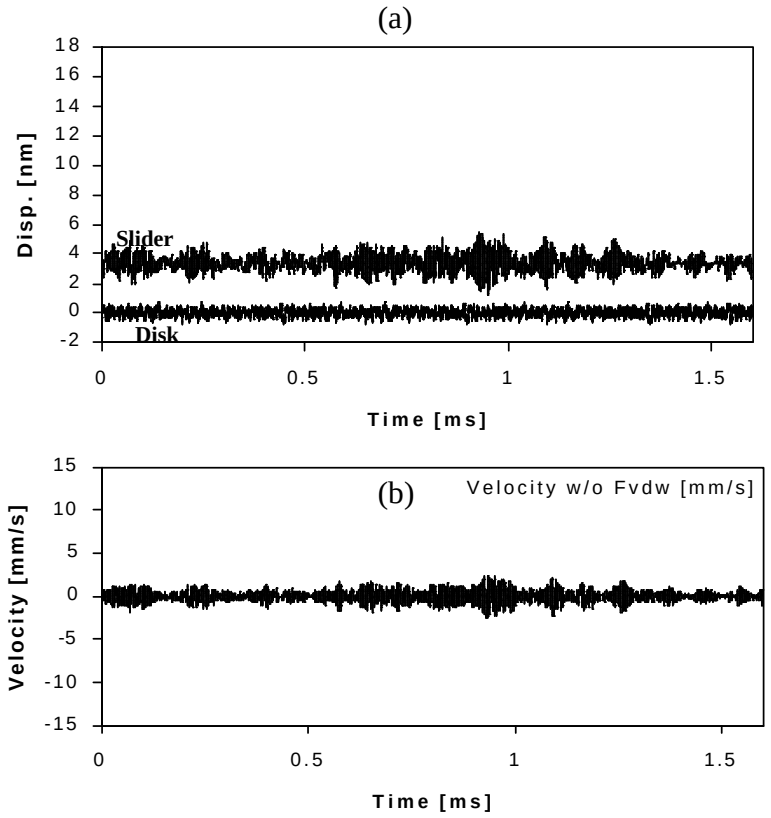

Fig. 21. Forced constant FH_{ss} simulation without including the intermolecular adhesion force showing the (a) disk and the sliders displacement and (b) the sliders velocity as functions of time.

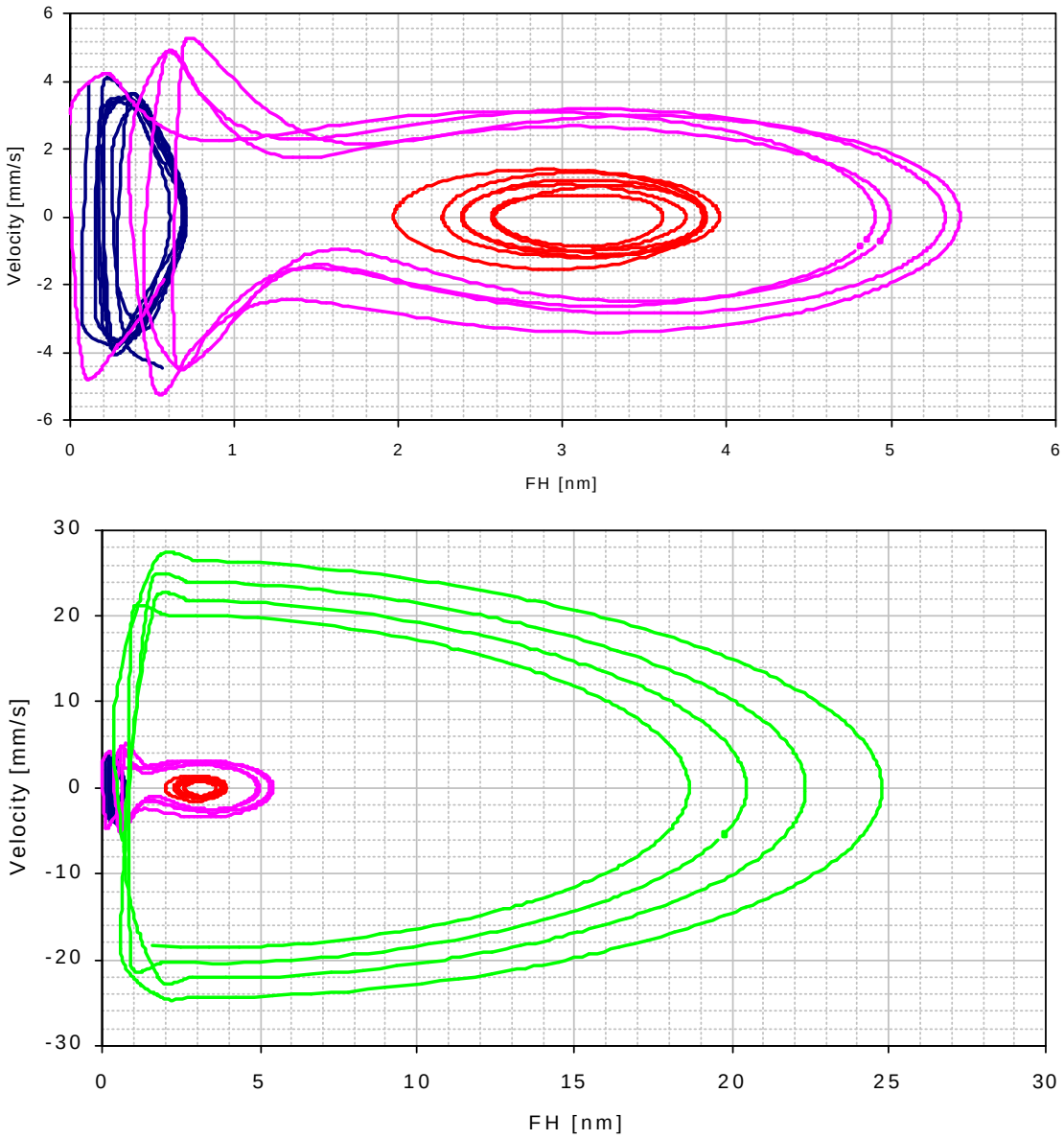

Fig. 22. The state-space trajectories for the forced system showing the different oscillation modes.

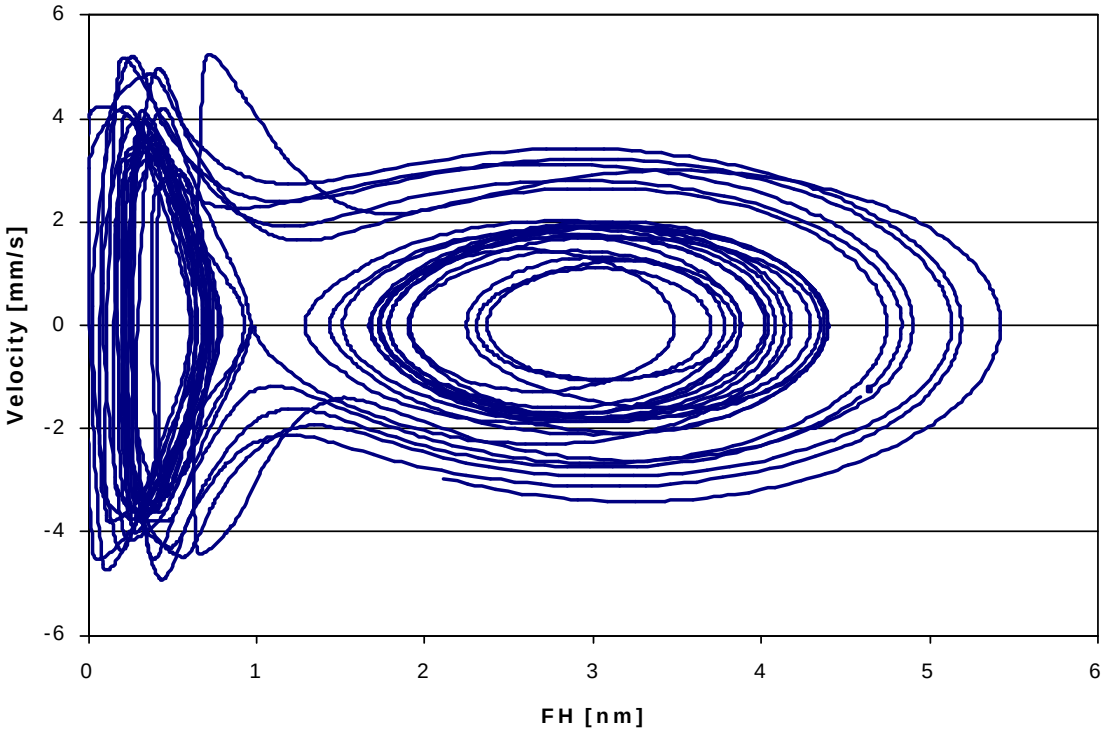

Fig. 23. The state-space trajectories for the forced system showing the switching between all oscillation modes randomly or chaotically.

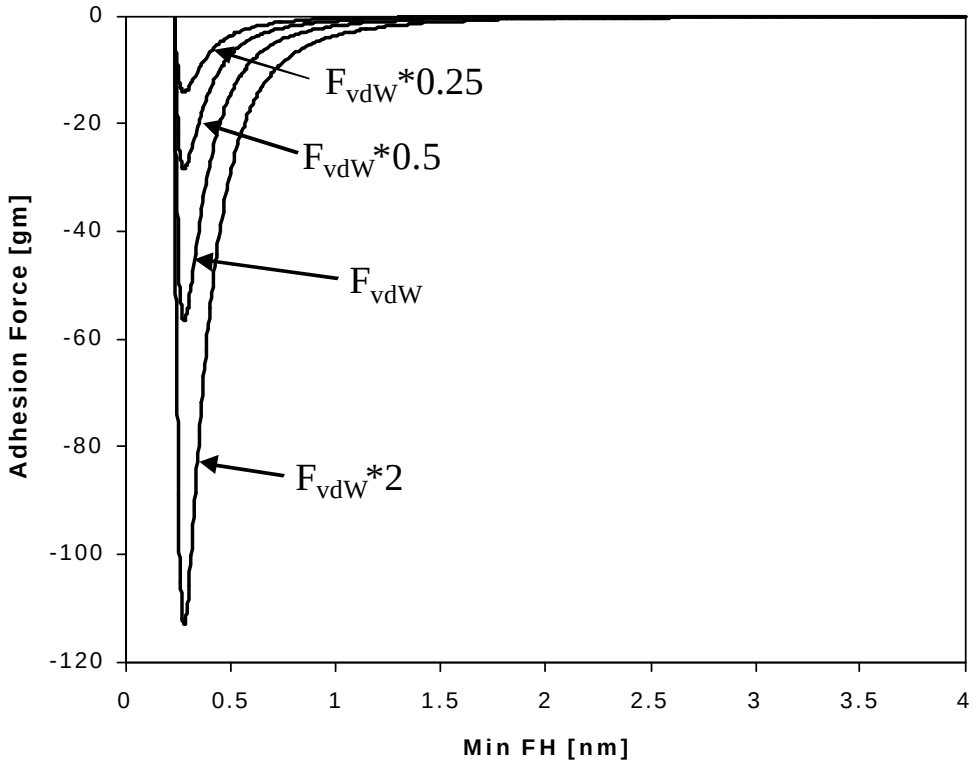

Fig. 24. Intermolecular adhesion forces used in the parametric study.

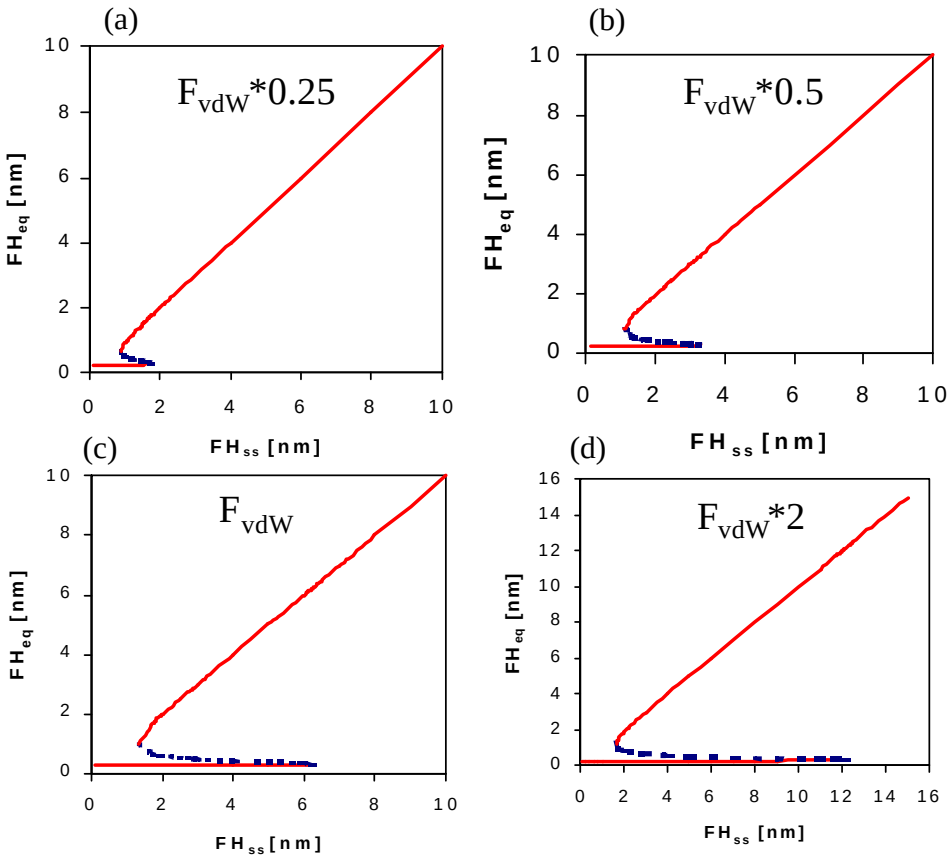

Fig. 25. Bifurcation plots for intermolecular adhesion forces equal to (a) F_{vdW}*0.25, (b) F_{vdW}*0.5, (c) F_{vdW}*1, and (d) F_{vdW}*2. (–) stable, and (- -) unstable.

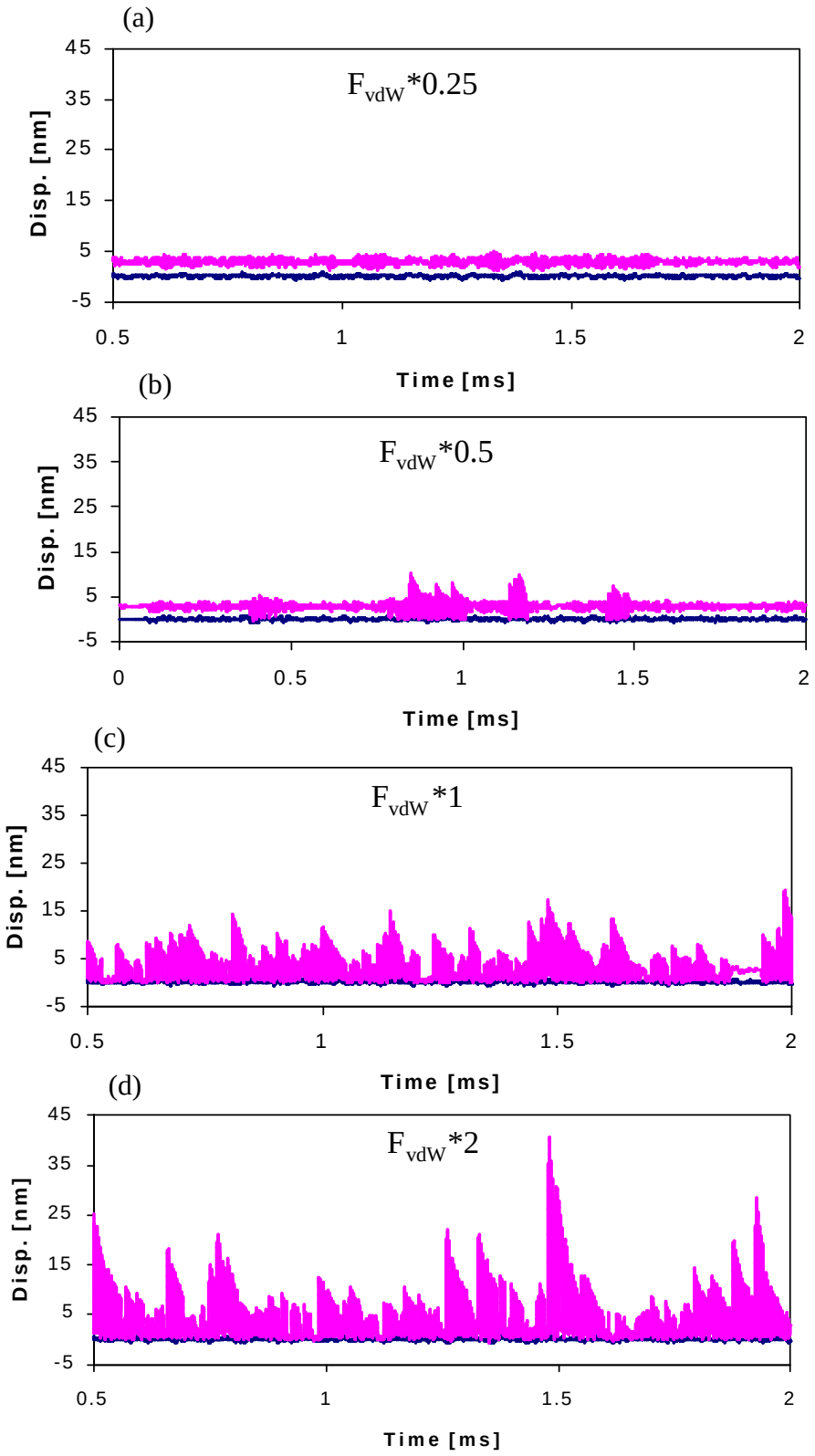

Fig. 26. Constant FH_{ss} simulations for intermolecular adhesion forces equal to (a) F_{vdW}*0.25, (b) F_{vdW}*0.5, (c) F_{vdW}*1, and (d) F_{vdW}*2.

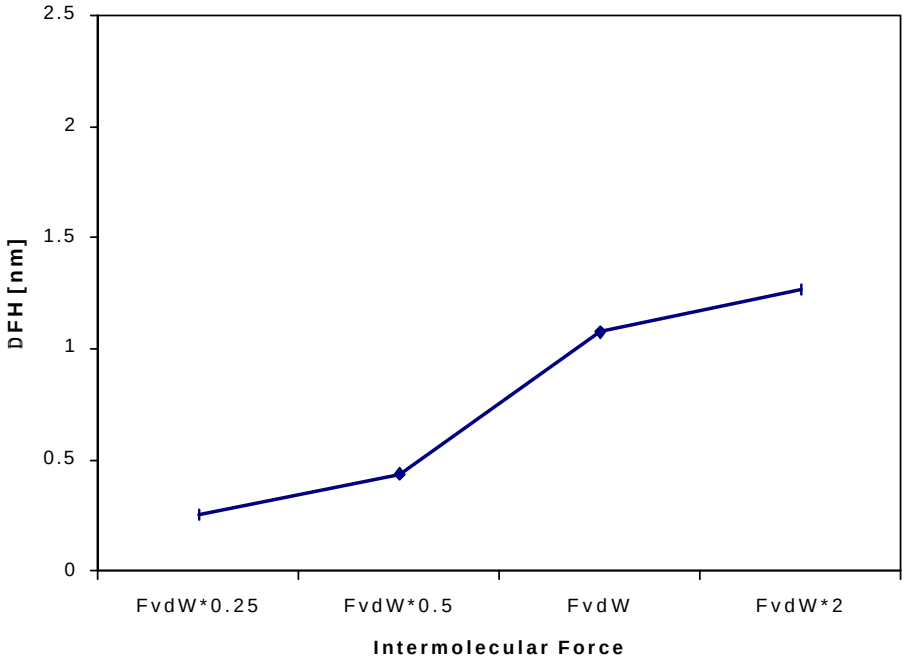

Fig. 27. FH hysteresis as a function of intermolecular adhesion force magnitude.

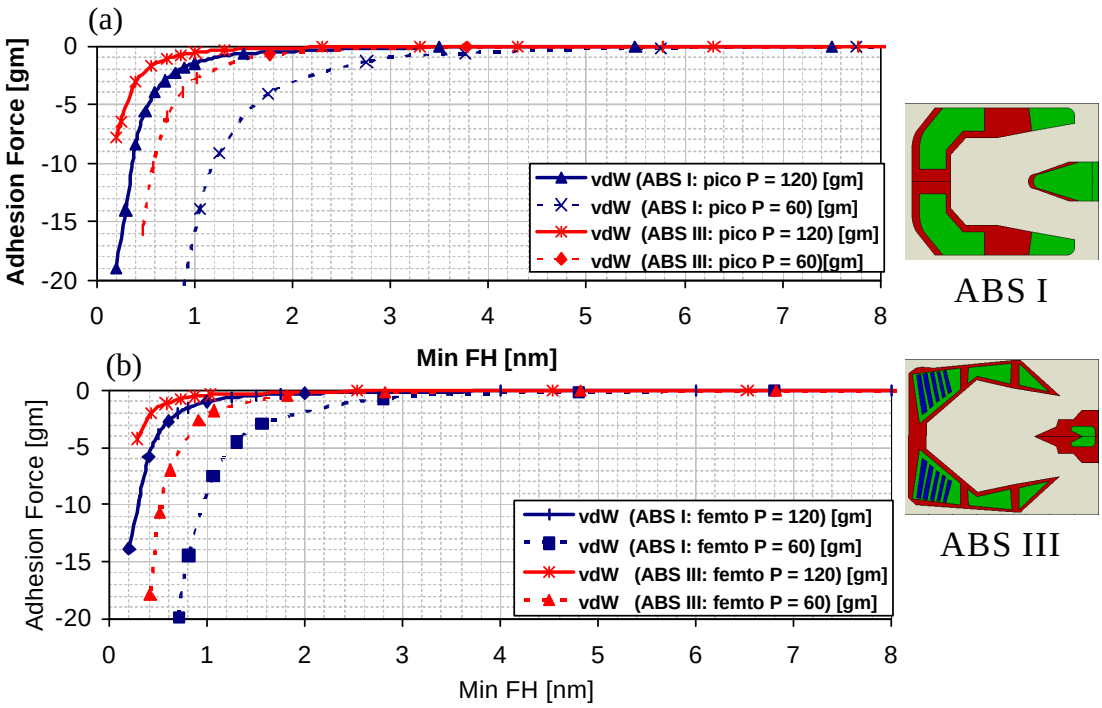

Fig. 28. Intermolecular adhesion force magnitude as a function of minimum spacing for (a) pico and (b) femto form-factors for two different ABS designs and two different pitch attitudes.

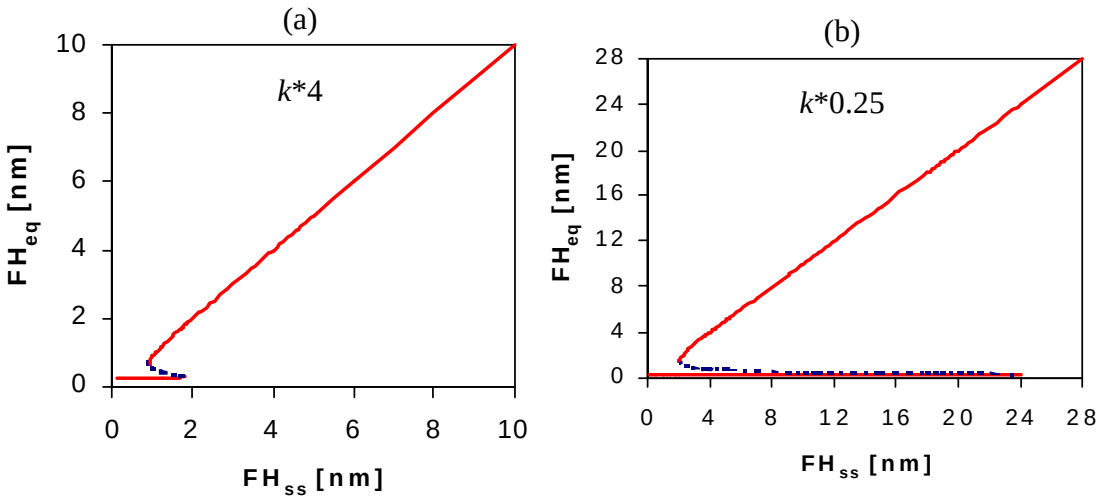

Fig. 29. Bifurcation plots for the nonlinear air bearing stiffness equal to (a) k*0.25, (b) k*4. (–) stable, and (- -) unstable.

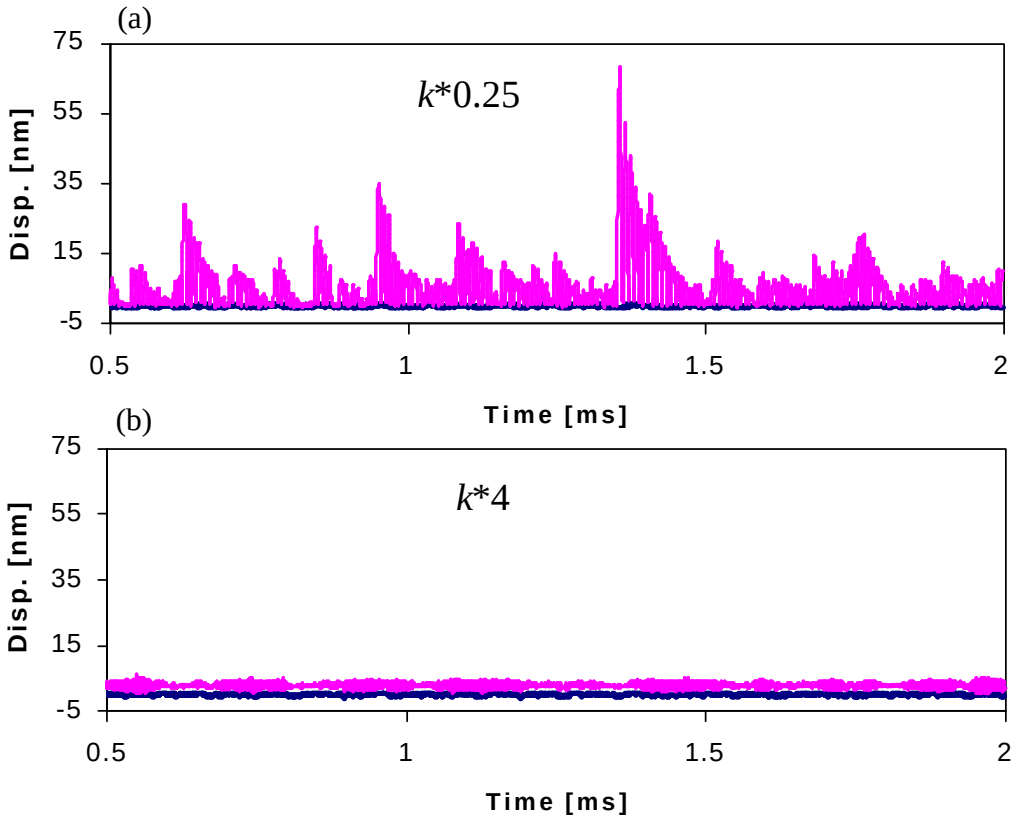

Fig. 30. Constant FH_{ss} simulations for the nonlinear air bearing stiffness equal to (a) k*0.25, (b) k*4.

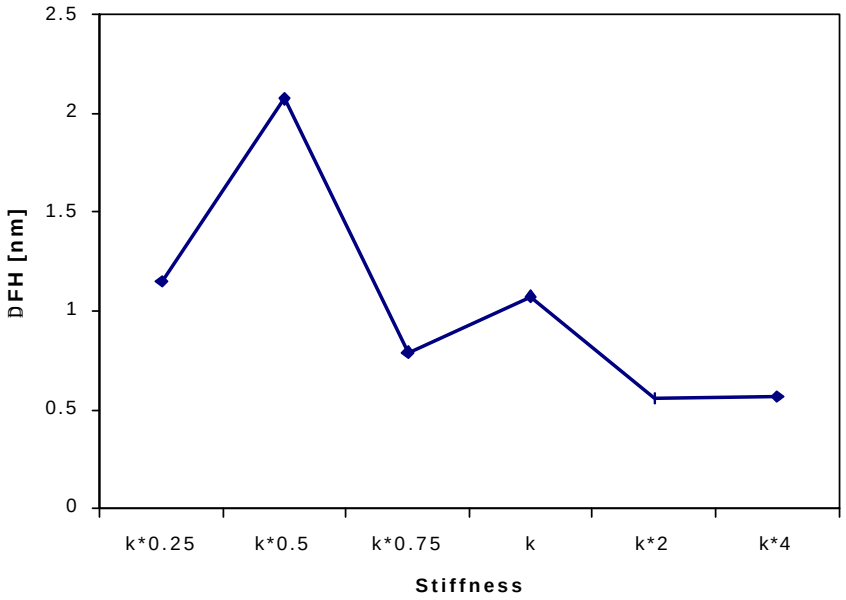

Fig. 31. FH hysteresis as a function of the nonlinear air bearing stiffness.

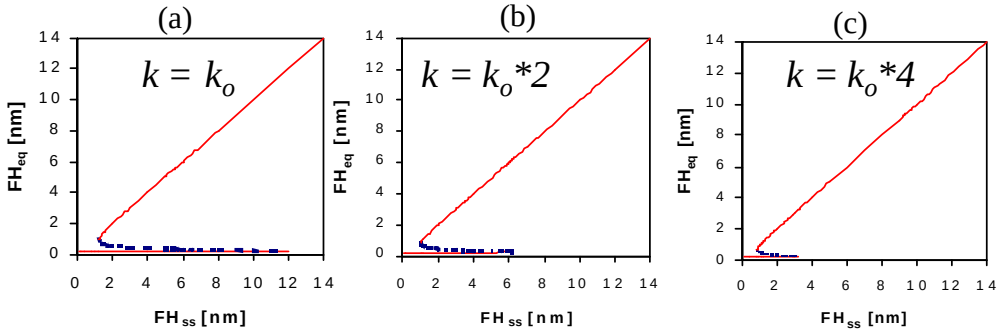

Fig. 32. Bifurcation plots for the linear air bearing stiffness equal to (a) k_o, (b) k_o*2 and (c) k_o*4. (–) stable, and (- -) unstable.

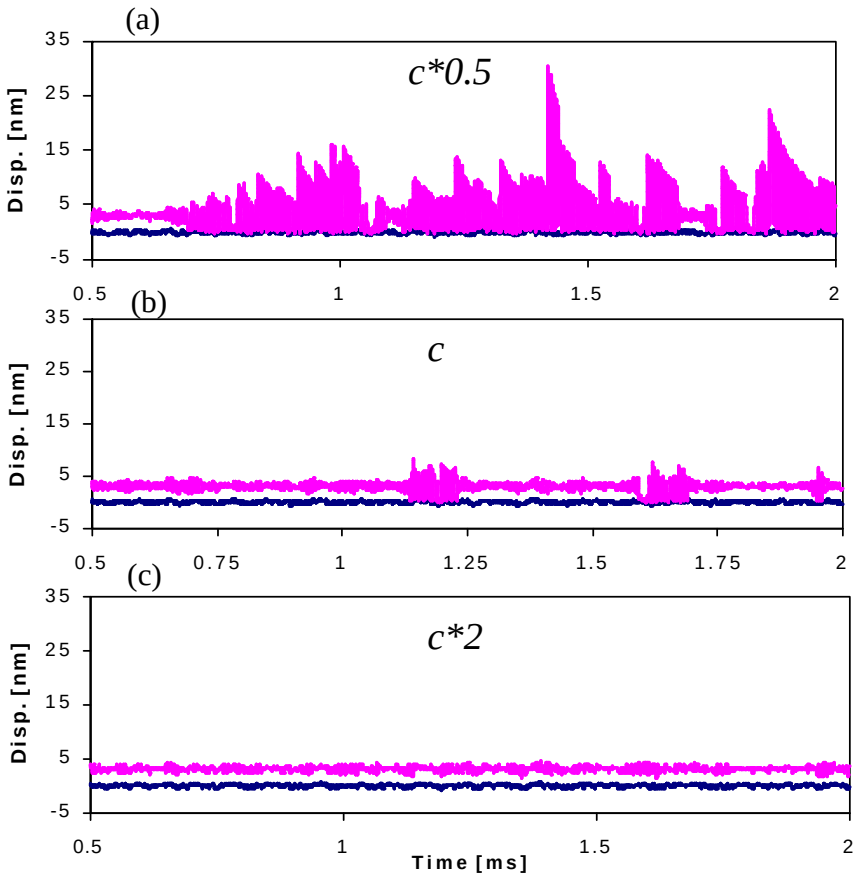

Fig. 33. Constant FH_{ss} simulations for air bearing damping equal to (a) *c*0.5*, (b) *c*, and (c) *c*2*.

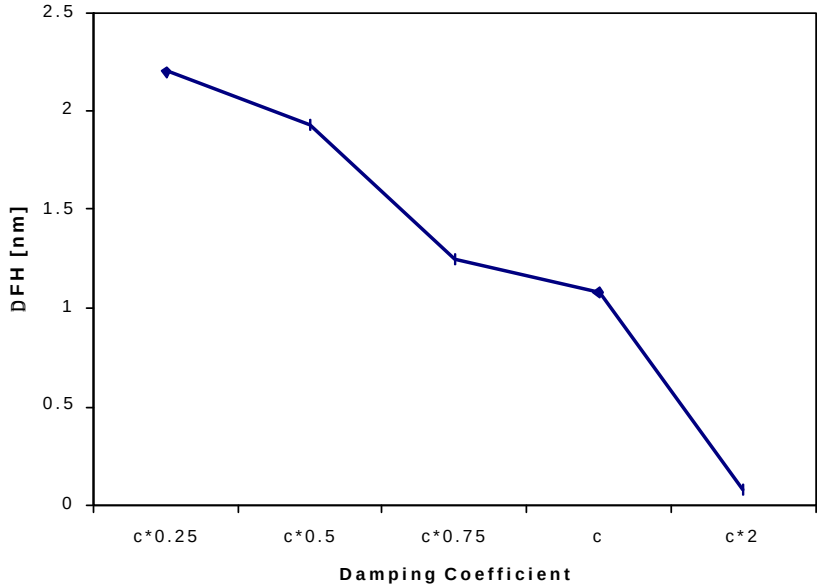

Fig. 34. FH hysteresis as a function of air bearing damping.

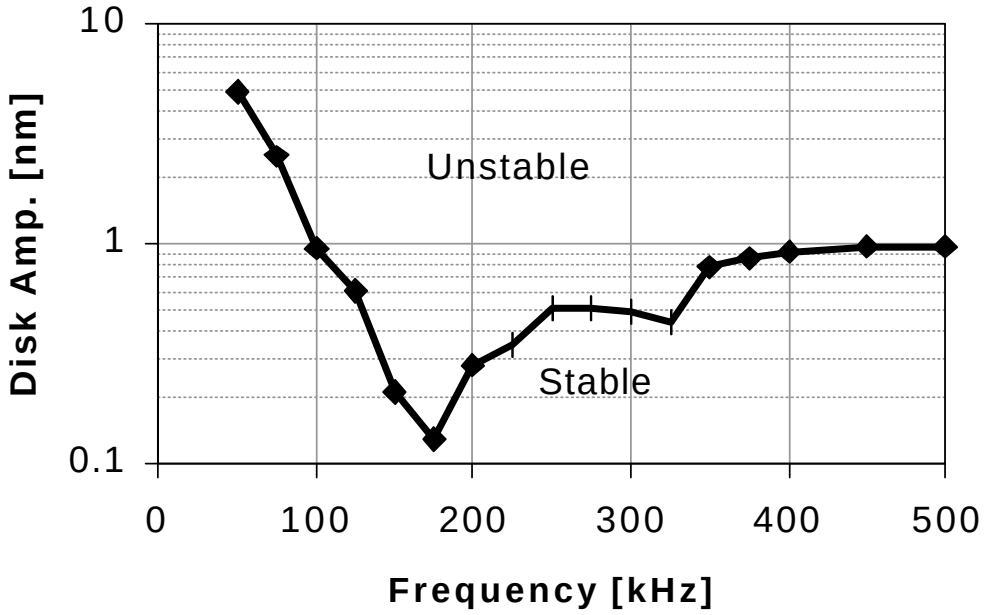

Fig. 35. Stable - unstable boundary for harmonic disk excitation.

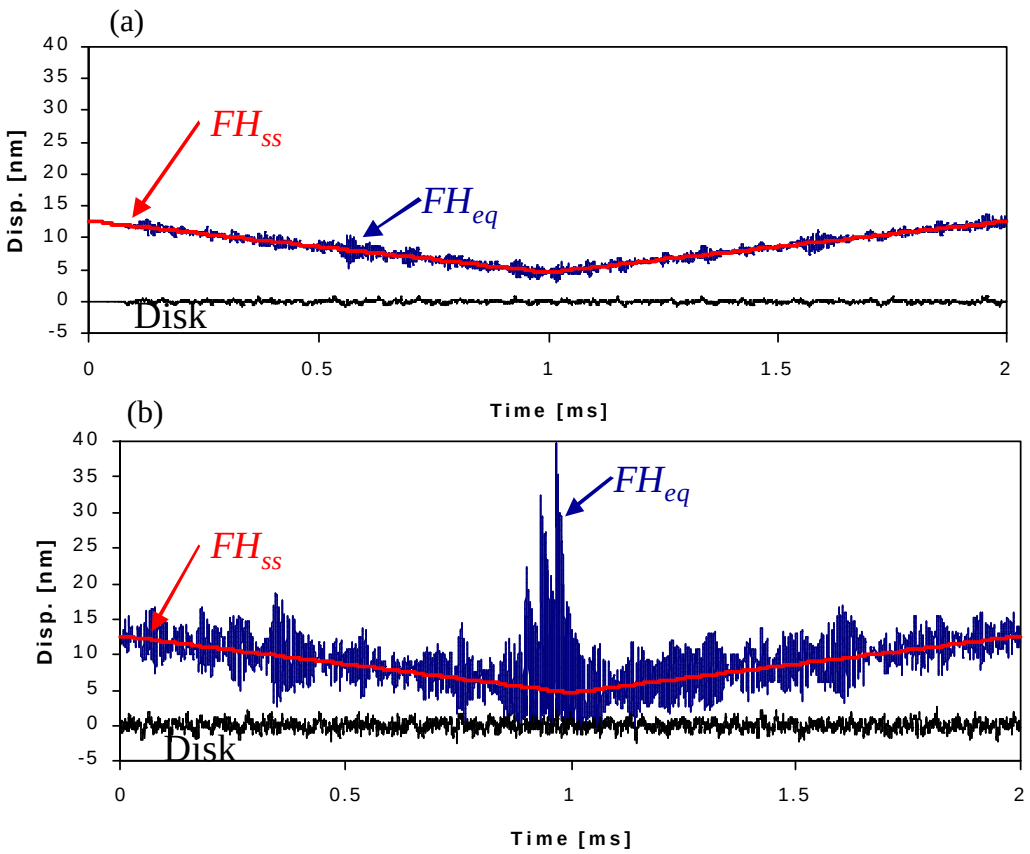

Fig. 36. TD-TO simulations forced by (a) disk A and (b) disk B.

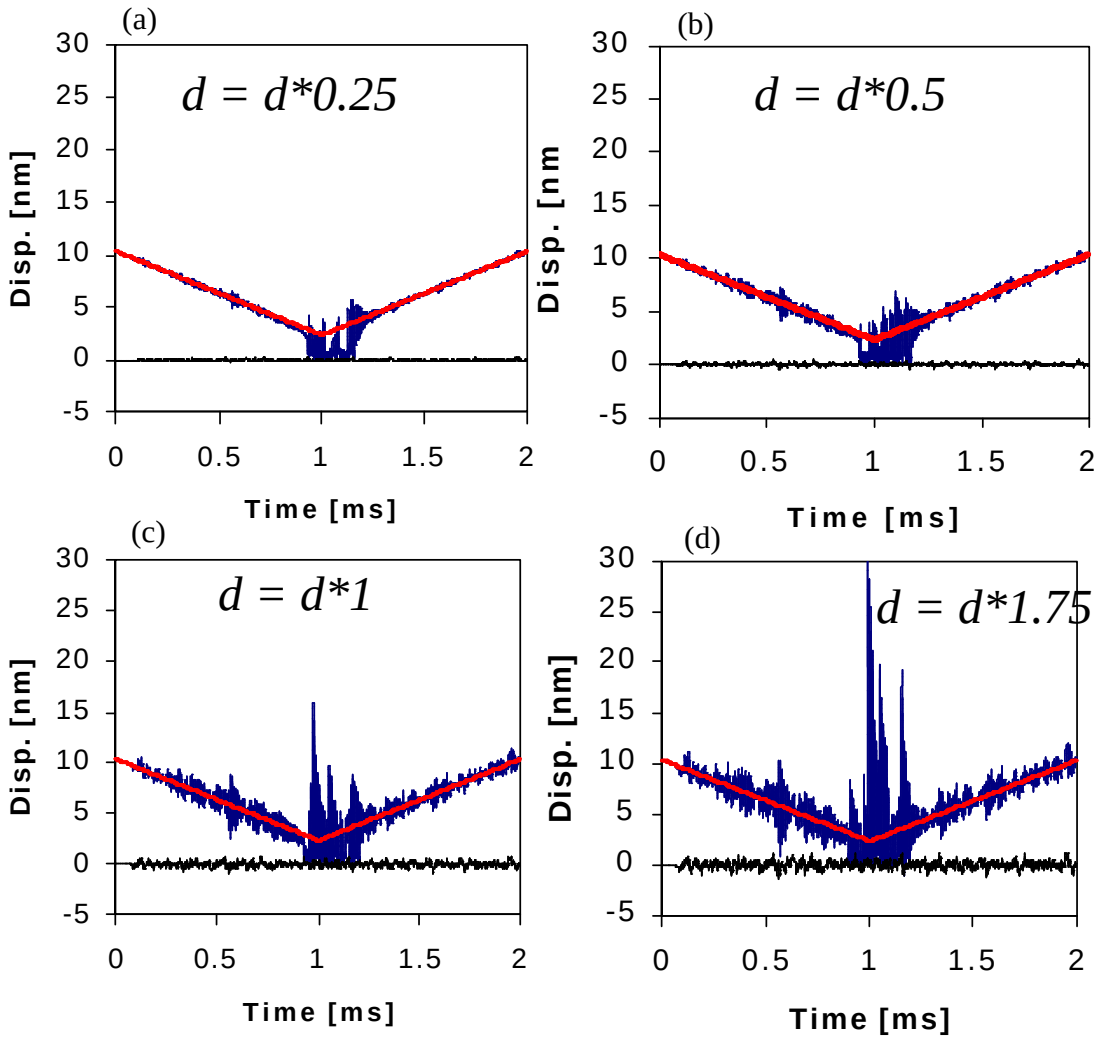

Fig. 37. TD – TO simulations by forcing the slider by disk A multiplied by: (a) 0.25, (b) 0.5, (c) 1, and (d) 1.75.

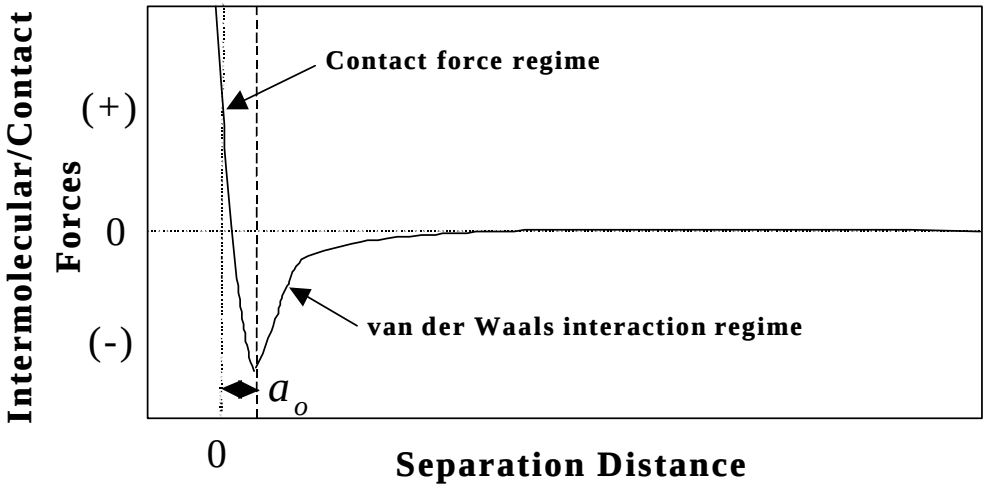

Fig. 38. Additional force generated by including the DMT model.